NASA
Technical
Paper
2626

August 1986

Testing of UH-60A Helicopter Transmission in NASA Lewis 2240-kW (3000-hp) Facility

Andrew M. Mitchell,
Fred B. Oswald,
and Harold H. Coe

NASA

Testing of UH-60A Helicopter Transmission in NASA Lewis 2240-kW (3000-hp) Facility

Andrew M. Mitchell,
Fred B. Oswald,
and Harold H. Coe

Lewis Research Center
Cleveland, Ohio

Summary

The U.S. Army's UH–60A Black Hawk 2240-kW (3000-hp) class, twin-engine helicopter transmission was tested at the NASA Lewis Research Center. The vibration and efficiency test results will be used to enhance the data base for similar-class helicopters. Most of the data were obtained for a matrix of test conditions of 50 to 100 percent of rated rotor speed and 20 to 100 percent of rated input power. The transmission's mechanical efficiency at 100 percent of rated power was 97.3 and 97.5 percent with its inlet oil maintained at 355 and 372 K (180 and 210 °F), respectively. The highest vibration reading was 72 g's rms at the upper housing side wall. Other vibration levels measured near the gear meshes are reported.

Introduction

Mission flight performance demands on advanced and future helicopters are increasing in severity. There exists the need to concurrently improve the power drive train's operational life and its mechanical efficiency (refs. 1 to 3). Elements contributing to mechanical efficiency and to vibration in lighter weight advanced geared systems are overviewed in reference 4 along with the related test data on the YUH–61A transmission. NASA Lewis tested the UH–60A helicopter transmission with the objective of adding to the existing technological data base. Mechanical efficiency and vibration data (two useful indicators in the design appraisal and monitoring of transmissions) were obtained under a matrix of operating conditions. Total input power ranged from 20 to 100 percent of rated at output rotor speeds from 50 to 100 percent of rated with oil inlet temperatures of 355 and 372 K (180 and 210 °F). Vibration results are presented as Fourier spectra and acceleration levels.

Apparatus

Test Transmission

The UH–60A helicopter transmission has a twin-engine input power rating of 2110 kW (2828 hp), an output rotor speed of 258 rpm, and a tail output shaft speed of 4117 rpm. The transmission is designed to provide the 81.042:1 speed reduction required (engine to rotor output) directly without external speed reduction units and also a 5.078:1 speed

reduction for the tail output shaft. The housing material is a magnesium alloy. The transmission's flight configuration weighs 565 kg (1245 lb). It was tested at Lewis with its flight oil cooler, blower, and forward accessory units detached from the input modules.

The UH–60A transmission (figs. 1 and 2) consists of two input modules and one main module (which includes the accessory modules). In each input module a 22-tooth spiral-bevel input pinion drives an 80-tooth spiral-bevel input gear. This gear rotates with an internal overrunning ramp roller clutch and transmits power through the shaft to the forward accessory module's bevel drive gear. This shaft also connects to the second-stage, 17-tooth combining bevel pinion driving an 81-tooth gear, which is splined to a 62-tooth sun gear. The sun gear drives five 83-tooth planetary gears, with the carrier splined to the output rotor shaft. The stationary ring gear has 228 teeth. The upper main bevel 116-tooth gear drives the 34-tooth tail output shaft pinion. Total reduction is

$$\frac{80}{22} \times \frac{81}{17}\left(1 + \frac{228}{62}\right) = 81.042$$

Shaft speeds, gear tooth numbers, and gear and vibration frequencies are shown in table I(a).

Two (duplex) hydraulic pumps are driven by a gear attached to the planetary carrier. They provide pressurized lubrication and oil scavenging for the two input modules and the main module. The lubricant was a type II commercial turbine engine oil, a mixture of 98 percent pentaerythritol (PE) and 2 percent depentaerythritol (DPE) ester.

Test Facility

The NASA Lewis 2240-kW (3000-hp) helicopter transmission test facility (figs. 3 and 4) consists of three regenerative (four square) testing power-flow loops (two inputs and a single tail power-out loop), all recirculating through the main rotor. Shaft speed is provided by a constant-speed 600-kW (800-hp) induction motor, and speed is controlled by an eddy current clutch. Power in each loop is remotely induced by a two-stage, planetary-geared torquer. Since power flow is recirculating, only frictional losses need be replenished by the drive system (ref. 4).

Immediately above the transmission is the rotor loader assembly, which is connected to the transmission's output rotor shaft. The loader assembly housing is attached to three vertical hydraulic cylinders positioned above it and located at the

apexes of an equilateral triangle. A fourth cylinder is attached and reacts horizontally. Controlling the cylinder pressures produces reaction through to the transmission's output shaft to simulate flight lift, two-axis moment, and drag (horizontal) load during testing. During operational testing the input speeds, torques, and rotor loads are controlled from a remote control room.

The output rotor shaft speed is measured by an inductive speed pickup. Input and tail rotor torque are measured, controlled, and displayed by a telemetry torsion measurement system through strain gauge bridges on the rotating input shafts. The system was calibrated at torque intervals by the deadweight moment method.

The facility's lubrication system consists of two pumps rated at 0.66 m³/min (173 gal/min) and 690 kPa (100 psi) flowing through three tube-and-shell oil/water heat exchangers located above the sump. The heat exchangers supply temperature-controlled oil to the facility's gearboxes and torquers. Ten-μm filters are installed in each lubrication output branch. Lubrication oil temperature and pressure sensors to all facility gearboxes and torquers are connected to limit-warning annunciators. The facility was lubricated with a commercially available turbine-quality mineral oil.

The water system from the cooling towers is at 586 kPa (85 psi) and supplies water for the dynamic clutch and the facility oil/water heat exchangers.

Four television cameras allow control room monitoring of the facility during testing. Upon annunciator warning the CO_2 "cell flood" system can be manually activated.

The NASA Lewis data acquisition system, Escort II, supports steady-state experimental facilities at the Center (fig. 5). Escort II, through individually dedicated minicomputers, has real-time data acquisition and processing capability for up to 256 measurement channels while maintaining a 2- to 3-sec update rate of facility displays. Mainframe computing capabilities are also available in the off-line batch mode.

Procedure

Efficiency

The test transmission (fig. 6) was thermally insulated to provide an adiabatic enclosure for the efficiency tests. The insulation package consisted of 25- to 100-mm (1- to 4-in.) thick fiberglass blankets (fig. 7) covered with an aluminized coated asbestos cloth enclosing the transmission. Sheet metal housed the transmission, with the exception of the top. The transmission had minor heat losses through the annuli of the input shafts and the tail output shaft and by convection and radiation from the housing and the insulation. Twenty-four Chromel/Alumel, type K, thermocouples were placed on the housing and on top of the upper insulation blankets. One thermocouple was also placed in each shaft annulus to allow calculation of heat losses from the housing.

The testing consisted of varying the output speed and torque through the matrix of set points shown in table II. Input power levels for efficiency tests ranged from 19 to 98 percent of rated power at nominal output rotor speeds of 50, 75, and 100 percent. For each data point the specified torque and speed were set and the transmission was operated at that setting until all temperatures had reached equilibrium. Equilibrium was assumed to have been achieved when no temperature had changed more than 1 deg K (2 deg F) in 10 min. The oil inlet temperature was maintained at 355 K (180 °F) for one series of tests and at 372 K (210 °F) for a second series. Data taken included oil inlet and outlet temperatures and mass flow rates through the oil/water heat exchanger, the speed and torque of the input shafts, and the surface temperatures of the transmission's enclosure. Transmission power loss, input power, and housing heat loss were determined. The mechanical efficiency of the transmission was calculated by

$$E = \frac{P_i - (P_1 + P_2)}{P_i} \times 100$$

where

E mechanical efficiency, percent

P_i transmission input power

P_1 transmission mechanical power loss to heat exchanger

P_2 heat convection and conduction power loss through housing and shafts

The total transmission power loss was determined to be the sum of the heat transferred to the oil and the heat lost to the surrounding air. The heat transferred to the oil was calculated from the oil flow rate and the temperature change through the heat exchanger. The heat lost to the surrounding air was calculated as the sum of the convective losses from the three rotating shafts and the natural convective losses from the surfaces of the transmission's enclosure. The radiation losses were negligible (refs. 5 and 6).

Vibration

Eleven piezoelectric accelerometers, designated as (VIB's), were fitted to various locations on the transmission's housing (fig. 8). The sensitivity of the accelerometers was ±5 percent at 2 to 5500 Hz and +20 percent at 10 kHz. The resonant frequency was 27 kHz.

In the vibration measurement system (fig. 9) accelerometer output was fed to vibration meters (charge amplifiers) that produced a dc output representing the overall peak acceleration level. The dc signal was converted to digital format for processing by the Escort II system. The vibration meters also produced an ac output signal that was stored on 14-channel

tape for analysis on a Fourier analyzer. The vibration measurement system, excluding accelerometers, was calibrated by means of signal injection applied at the transmission. The accelerometers and the system were checked by a shake table.

Vibration data were acquired at various combinations of speed and torque (table II) from 13 to 100 percent of rated power. The tail torque was maintained throughout testing such that 16 percent of the total input power flowed out through the tail output shaft.

Frequency domain spectra were plotted from a Fourier analyzer by using a flat-top weighting window and a 0- to 10-kHz frequency span, at which the frequency resolution (bandwidth) is 95 Hz. When more accurate frequency measurement was required, zoom spectra were taken, improving frequency resolution to within 1 Hz.

Post-Test Inspection

At the conclusion of efficiency and vibration testing the transmission was removed from the test stand and disassembled to allow visual inspection at the component level. Oil samples were taken for oil particulate analysis. Chip detectors, filters, and the interior surfaces of the transmission's main housing were also visually inspected. The power train gearing components were photographed. Gear teeth adjacent to any gear tooth contact patterns (footprints) to be observed were whitened to highlight the footprints by light reflectance.

Results and Discussion

Efficiency

In the efficiency test 22 data points were taken for the matrix of rated speeds and input torques given in table II. The resulting power levels are also shown in the table. The transmission oil's inlet temperature was maintained constant at 355 K (180 °F) for readings 61 to 72 and at 372 K (210 °F) for readings 73 to 84. The results are shown in figures 10 to 12.

Figure 10 shows the transmission's mechanical efficiency as a function of input power for three nominal output shaft speeds for both oil temperatures. Figure 11 shows the efficiency at the same conditions as a function of the input torque. At the transmission's rated power level of 2110 kW (2828 hp) and rated output rotor speed of 258 rpm, the efficiency was 97.3 percent with 355 K (180 °F) oil and 97.5 percent with 372 K (210 °F) oil. The efficiency calculations showed that over 99 percent of the transmission power loss was contained in the heat transferred to the oil and that less than 1 percent of the losses were transferred by convection and conduction.

For a given input speed the efficiency was very high at the higher power or torque levels and diminished significantly at lower levels. At a given power or torque the efficiency went

up as the speed was reduced. This is to be expected since most of the power losses in a transmission, such as bearing friction, lubricant churning, gear meshing (elastohydrodynamic rolling traction), sliding, and windage, are speed dependent (refs. 4, 7, and 8). At a constant speed the changes in these power losses are much less than the change in power level as the torque is decreased. Since the losses then become a larger portion of the input power, the efficiency decreases. Likewise, at a given power level these losses would be smaller as shaft speed is reduced, thus increasing the efficiency. Also at constant speed, as the power or torque is steadily reduced to very low values, the input power approaches the tare (no load) losses, and the efficiency decreases very rapidly.

Power losses due to lubrication are a function of lubricant viscosity and density (ref. 9). At the higher oil temperature of 372 K (210 °F) the viscosity and density were lower, resulting in smaller power losses in the bearings and gear meshes, and thus higher efficiency. At the design point (100-percent speed and 100-percent torque) the increase in efficiency between the lower (355 K) and higher (372 K) temperatures was 0.2 percent, which is consistent with previous NASA Lewis test programs (refs. 4 and 10).

The dependence of efficiency on speed is further illustrated in figure 12, where efficiency is shown as a function of rotor speed for four values of input torque. The efficiency, as expected, decreased with increasing speed for a given torque. Thus, as speed was increased, the power losses increased at a faster rate than the input power. This was especially noticeable at the lowest torque (25 percent of rated). At this torque the lubrication regime tends toward hydrodynamic, where power losses are torque (load) sensitive. At full rated design speed and torque the lubrication regime is elastohydrodynamic, power losses are nearly torque insensitive, and the efficiency is an inverse function of the film thickness (refs. 11 and 12). Nevertheless, this UH–60A transmission is very efficient, considering the high-speed input stage gearing (20 900 rpm) and the large overall speed reduction (81:1).

Vibration

Gear vibration is caused by nonuniform action (transmission error) of the gear teeth as they roll through the mesh. Mark (ref. 13) reviews and defines the mean and random components of transmission error. The mean component (same for all teeth) is due to deviation of the average tooth surface from a perfect involute (conjugate) shape. These deviations are caused by manufacturing errors as well as torque-dependent distortion (ref. 13 and 14). The mean component of transmission error produces vibration at the harmonics of the tooth meshing frequency. The random component of transmission error results in vibration at AM and FM sideband frequencies. Amplitude modulation (AM) sidebands are caused primarily by eccentricity (runout) of a gear shaft, which causes the depth of gear tooth engagement to vary as the gears rotate. Such

sidebands occur at frequencies equal to the meshing frequency plus or minus multiples of pinion or gear shaft rotational frequency. Frequency modulation (FM) sidebands may be excited by tooth spacing errors or by torsional vibration of gear shafts. The intermodulation of AM and FM excitation may produce additional sidebands (refs. 15 and 16).

Any rigid body constrained by elastic supports will have natural vibration modes at frequencies determined by the system's effective mass and stiffness properties (ref. 17). A continuous structure will also have an infinite number of flexible body modes (independent of support conditions), some of which change frequency as rotational speed changes. In practice, however, one need not be concerned with modes of frequency higher than the first two to three harmonics of the highest excitation frequency (ref. 18).

The dc vibration signals processed by the Escort II system are plotted in figure 13. Each data point shown is an average of up to five measurements taken under similar (within 5 percent) conditions of speed and torque. The vibration level is generally strongly dependent on speed. VIB's 3, 4, and 7 are also strongly dependent on torque.

Vibration spectra from each of the 11 accelerometers (VIB's) are shown in figures 14 to 24 and are reported to within ±25 Hz. (Locations of the VIB's are shown in fig. 8.) Each figure includes three individual spectra (each spectrum rms averaged from 10 samples) and a speed map (each trace rms averaged from four samples). The spectra were taken under conditions of (1) 99-percent speed, 99-percent torque; (2) 75-percent speed, 100-percent torque; and (3) 94-percent speed, 74-percent torque. The speed maps were each obtained at 25-percent torque and at rotor speeds from 50 to 267 rpm (19 to 103 percent).

VIB 1.—VIB 1 was located on the top surface of a small projection from the main housing that contains the oil jets for the tail drive gear. This projection is near the upper roller bearing on the output (rotor) shaft. The vibration meter reading at 100-percent power (100-percent speed and 100-percent torque) for VIB 1 was 17 g's rms. The vibration amplitude (fig. 13(a)) was speed dependent and slightly torque dependent. The spectral traces (fig. 14) reveal frequency lines from planetary and main bevel gear meshes. There is a prominent line at 25 times (25 orders) the rotational frequency of the intermediate-speed shaft. (At 100-percent speed 2396 Hz is 25 times the frequency of the 5750-rpm intermediate-speed shaft.)

VIB 2.—VIB 2 was located on the flange of the ring gear between the left and rear mounting feet. The sensitivity axis of VIB 2 was radial to the ring gear. The vibration meter reading at 100-percent power was 17 g's rms. The vibration amplitude (fig. 13(b)) was speed dependent and moderately torque dependent. Spectral traces (fig. 15) are dominated by planetary harmonics. (At 100-percent speed the lowest planetary frequency was 980 Hz.)

VIB 3.—VIB 3 was located on the top surface of the left input module above the bearings (one ball, one roller) at the

heel end of the high-speed input pinion. The vibration meter reading at 100-percent power was 49 g's rms. The vibration amplitude (fig. 13(c)) was strongly dependent on both speed and torque except for readings taken at 75-percent speed, which show little torque effect. The spectral traces for VIB 3 (fig. 16) are dominated by a line at 2396 Hz (100-percent speed). This is 25 orders of the rotational speed of the intermediate-speed shaft (as noted for VIB 1). The input gear meshing frequency (first reduction) at 7667 Hz (100-percent speed) is also prominent along with a sideband at three times the high-speed-shaft frequency (348.5 Hz at 100-percent speed) above 7667 Hz. Two intermodulation frequencies have been identified in figures 16(a) and (c): (1) a strong line at 9925 Hz (at 99-percent speed), which is the sum of the input gear meshing at the 7667- and 2396-Hz lines and (2) a line at 5200 Hz (at 99-percent speed), which is the difference between the 7667- and 2396-Hz lines.

VIB 4.—VIB 4 was located on the top surface of the left input module directly above the 80-tooth input gear/freewheel assembly. The vibration amplitude (fig. 13(d)) was strongly affected by speed and torque. The spectra (fig. 17) for VIB 4 show a very strong line at the input gear meshing frequency (7667 times percent speed). The 25 orders of intermediate-speed-shaft lines appear in the traces of figure 17 along with lines at the sum and difference of the input gear meshing frequencies (7667 ± 2396 Hz at 100-percent speed). There is also a prominent line (3485 Hz at 100-percent speed) at 10 orders of the input (high speed) shaft frequency.

VIB 5.—VIB 5 was located on the top surface of the main housing just above the tapered roller bearing at the heel end of the left combining spiral-bevel pinion gear. The vibration meter reading at 100-percent power was 14 g's rms (fig. 13(e)). The spectra (fig. 18) show several harmonics of planet gear meshing (n times 980 Hz times percent speed, n = 1,2,...) and main bevel gear meshing (1629 Hz times speed). The speed map (fig. 18(d)) reveals a mild resonance at 6300 Hz, excited by the high-speed mesh at 210-rpm (81 percent) rotor speed.

VIB 6.—VIB 6, located on the front mounting foot, gives an indication of vibration transmitted to the airframe of an actual helicopter. The vibration meter reading at 100-percent power was 6 g's rms (fig. 13(f)). The spectra (fig. 19) show, at very low vibration levels, the lower harmonics of the planet gears and main bevel gear meshing.

VIB 7.—VIB 7 was located on the top surface of the right input module (comparable to VIB 3). The vibration meter reading at 100-percent power (fig. 13(g)) was 41 g's rms. The levels were lower and slightly less speed dependent than those of VIB 3. The spectra (fig. 20) are dominated by a very strong line (30 g's at a nominal 100-percent power) at the input gear meshing frequency (7667 Hz) and by strong sidebands spaced at multiples of the high-speed-shaft frequency (348.5 Hz) from the carrier frequency. The sidebands indicate runout (eccentricity) in the high-speed (20 909-rpm) shaft. At an output rotor speed of 150 rpm (58 percent) the speed map (fig. 20(d)) shows

a small resonance at 4400 Hz, excited by the input mesh. At 140 to 150 rpm there was also some response at 8500 to 9000 Hz, excited by the second harmonic of input mesh. The enhanced response at 9000 Hz contributes to the upper sidebands of the input gear meshing frequency at 100-percent speed.

VIB 8.—VIB 8 was located above the right input gear (comparable to VIB 4). The vibration meter reading at 100-percent power was 18 g's rms (fig. 13(h)). The amplitude was much lower and much less sensitive to speed and torque than that for VIB 4. The spectral traces (fig. 21) show very little response at frequencies above 5 kHz. A resonant condition at 1800 Hz, seen in the speed map (fig. 21(d)), was excited by the input gear meshing frequency at 60-rpm (23 percent) rotor speed and by the 25 orders of intermediate-speed-shaft frequency at 190 rpm (74 percent). This same 1800-Hz response caused a prominent line in the spectra at 75-percent speed excited at 25 orders of the rotational frequency of the intermediate-speed shaft (fig. 21(d)).

VIB 9.—VIB 9 was located on the top right side of the main housing (comparable to VIB 5). The vibration reading at 100-percent power was 23 g's rms (fig. 13(i)). The spectra (fig. 22) show a very strong line at the input gear meshing frequency (7667 Hz) along with sidebands spaced at the input shaft frequency (348.5 Hz). At a much lower level lines appear from several harmonics at the planet gear meshing frequency (980 Hz fundamental) and at the main bevel gear meshing frequency (1629 Hz fundamental at 100-percent speed).

VIB 10.—VIB 10 was mounted on the side wall of the main housing near the top and normal to the surface. The vibration meter reading at 100-percent power was 57 g's rms (fig. 13(j)). An even higher reading of 72 g's rms was recorded at 100-percent speed and 50-percent torque. VIB 10 was very speed sensitive. The speed map (fig. 23(d)) shows strong resonant response of the housing's side wall at 2200 Hz. The greatest response (72 g's rms) occurred at 230-rpm rotor speed (90 percent), excited by the 25 orders of intermediate-speed-shaft frequency described earlier (2396 Hz at 100-percent speed). Other frequency lines that show strongly in figure 23 are harmonics of the planet gear meshing frequency (980 Hz) and the main bevel gear meshing frequency (1629 Hz).

The very strong resonant response of the housing's side wall is expected to be a major contributor to the airborne noise produced by the gearbox. Acoustical measurements to determine sound power levels were not performed.

VIB 11.—VIB 11 was located on the housing above the tail output shaft gear. The vibration meter reading at 100-percent power was 15 g's rms (fig. 13(k)). The speed map (fig. 24(d)) shows strong response at about 1000 Hz, excited by the planet gear meshing frequency (980 Hz) especially at the highest rotor speed of 267 rpm (103 percent). The tail output shaft gear mesh excites the resonance slightly at 110 rpm (43 percent). Figure 24(b) (75-percent speed, 100-percent torque) shows the main bevel gear meshing frequency (reduced to 1222 Hz) to be strong because of the 1000-Hz resonance.

Overall, the vibration spectra (figs. 14 to 24) are dominated by shaft-related frequencies, such as gear meshing harmonics and low harmonics of shaft speed, and by their intermodulation products. As a general trend larger vibration amplitude is associated with the spiral-bevel gears than with the spur gears in the planetary stage. This is consistent with prior testing experience with transmissions of various sizes (refs. 2 and 4). Higher amplitude from the spiral-bevel gears might be expected in part because they are used in the high-speed first reduction stages of the transmission.

One of the most prominent vibration frequency lines for the UH–60A transmission was at 25 orders of the rotational frequency (2396 Hz at 100-percent speed) of the intermediate-speed shaft as observed at VIB's 1, 3, 4, and 10 (figs. 14, 16, 17, and 23). This frequency was much stronger on the left input module than on the identical right module. No component (gear or bearing) could be found in either the transmission's or the test facility's gearboxes that would produce vibration at the measured frequency. Another unexplained frequency is the 10 orders of high-speed-shaft frequency found in the spectra of VIB 4 (fig. 17).

To determine that the 2396-Hz spectral line is not caused by the tail output shaft gear (whose meshing frequency is 63 Hz lower at 2333 Hz), the tail output shaft was removed and the transmission was operated briefly. The only difference noted in the frequency content of the vibration spectra was the absence at VIB 11 of the 2333-Hz (tail output shaft gear) spectral line. The 2396-Hz line was still present.

A possible explanation for these frequency lines is that they may be so-called ghost frequencies caused by undulation errors produced by gear cutting or grinding machines. An example of ghost frequencies in helical gearing is given in reference 19. An inquiry of the manufacturer disclosed that there is a 25:1 reduction ratio in the gear train driving the work table of the gear grinding machine used for the 80-tooth gear on the intermediate-speed shaft. It is suggested that some type of rotational error transmitted through this 25:1 gear train may be the source of the 25-orders vibration. A similar machining error may be the cause of the 10-orders vibration.

Vibration frequencies produced by rolling-element bearing defects were calculated (ref. 20) and are listed in table I(b). None of the calculated bearing defect vibration frequencies match prominent lines in the spectra of figures 14 to 24. No attempt was made to find bearing passing frequencies among weaker spectral lines.

Post-Test Inspection

After 35 hours of efficiency and vibration testing the transmission was removed and disassembled for inspection. The transmission's lubrication oil was sampled for particulate analysis. There was no significant increase in contaminant level over new oil. Oil system component integrities were acceptable. The general overall appearance of all parts was indicative of moderate loading with no flaws or indications

of abnormal wear. Bearings and gear train components were also visually examined for any defects that could contribute to the 25 orders of the intermediate-speed shaft vibration levels observed. Possible specific contributory flaws were not observed. The input spiral-bevel gear teeth (fig. 25) displayed light surface wear and full gear tooth contact patterns. The unloaded side of the gear teeth displayed the manufacturer's gear tooth grinding marks, indicating no gear tooth contact on the unloaded sides.

Summary of Results

The U.S. Army's UH-60A Blace Hawk transmission was tested to determine its mechanical efficiency and vibration characteristics and spectra in order to supplement the operational data base for similar-class helicopters.

The following results were obtained:

1. The UH-60A helicopter transmission's mechanical efficiency at rated speed and load (258 rpm and 2110 kW) was 97.3 and 97.5 percent with oil inlet temperatures of 355 and 372 K (180 and 210 °F), respectively.

2. Vibration meter readings at 100-percent speed and torque generally ranged from 6 to 50 g's rms.

3. Much higher vibration levels, up to 72 g's rms, were measured at VIB 10 (located on the side wall of the main housing). The data indicate that the very high levels are largely due to a resonance condition of the side wall at 2200 Hz.

4. A strong (constant ratio) excitation was found at a frequency of 25 times the intermediate-speed-shaft rotational frequency (2396 Hz at 100-percent speed). At 90-percent speed (230 rpm) this frequency excited the 2200-Hz resonance observed at the housing's side wall.

5. At the right input module at rated speed and torque the high-speed gear stage produced a 30 g's rms line and the strong sidebands typical of runout.

6. Post-teardown visual inspection revealed only mild wear on all power train components and no visible surface faults correlatable to the high vibration levels observed.

National Aeronautics and Space Administration
Lewis Research Center
Cleveland, Ohio, May 6, 1986

References

1. Weden, G.J.; and Coy, J.J.: Summary of Drive Train Component Technology in Helicopters. Gears and Power Transmission Systems for Helicopters and Turboprops, AGARD CP-369, AGARD, 1985, pp. 2-1 to 2-17.

2. Zaretsky, E.V.; Coy, J.J.; and Townsend, D.P.: NASA Transmission Research and Its Probable Effects on Helicopter Transmission Design. Proceedings, 39th Annual Forum, American Helicopter Society, 1983, pp. 303-320.

3. Stevens, S.C.: AVRADCOM Research Helicopter Vibrations. Shock and Vibration Bulletin, no. 53, pt. 1, May 1983, pp. 3-20.

4. Mitchell, A.M.; Oswald, F.B.; and Schuller, F.T.: Testing of YUH-61A Helicopter Transmission in NASA Lewis 2240-kW (3000-hp) Facility. NASA TP-2538, 1986.

5. Marks, L.S.; and Baumeister, T., eds: Standard Handbook for Mechanical Engineers, 7th edition, McGraw-Hill, 1967, pp. 4-90 to 4-109.

6. Kleckner, R.J.; Dyba, G.J.; and Ragen, M.A.: Spherical Roller Bearing Analysis, SKF Computer Program, Vol. 2—User's Manual. (SKF Report No. AT81D007 and SKF Program No. AT81Y001, SKF Industries; NASA Contract NAS3-22807.) NASA CR-167859, 1982, pp. 108-113.

7. Anderson, N.E.; and Loewenthal, S.H.: Effect of Geometry and Operating Conditions on Spur Gear System Power Loss. J. Mech. Des., vol. 103, no. 1, Jan. 1981, pp. 151-159.

8. Anderson, N.E.; Loewenthal, S.H.; and Black, J.D.: An Analytical Method to Predict Efficiency of Aircraft Gearboxes. AIAA Paper 84-1500, June 1984.

9. Anderson, N.E.; and Loewenthal, S.H.: Spur-Gear-System Efficiency at Part and Full Load. NASA TP-1622, 1980.

10. Mitchell, A.M.; and Coy, J.J.: Lubricant Effects on Efficiency of a Helicopter Transmission. Problems in Bearings and Lubrication, AGARD CP-323, AGARD, 1982, pp.20-1 to 20-16.

11. Hamrock, B.J.; and Dowson, D.: Isothermal Elastohydrodynamic Lubrication of Point Contacts, Part III—Fully Flooded Results. J. Lubr. Technol., vol. 99, no. 2, Apr. 1977, pp. 264-276.

12. Jacobson, B.O.; Hogland, E.; and Hamrock, B.J.: Correlation of Rheological Characteristics of Lubricants with Transmission Efficiency Measurements. NASA TM-86988, 1985.

13. Mark, W.D.: Gear Noise Excitation. Engine Noise: Excitation, Vibration, and Radiation, R. Hickling and M.M. Kamal, eds., Plenum, 1982, pp. 55-94.

14. Houser, D.R.: Gear Noise Sources and Their Prediction Using Mathematical Models. Presented at the Original Equipment Manufacturer (OEM) Conference, Philadelphia, PA, Sept. 11, 1985.

15. Dale, A.K.: Gear Noise and the Sideband Phenomenon. ASME Paper 84-DET-174, Oct. 1984.

16. Gu, A.L.; and Badgley, R.H.: Prediction of Vibration Sidebands in Gear Meshes. ASME Paper 74-DET-95, Oct. 1974.

17. Stockton, R.J.: Sun Gear Traveling Wave Vibration in a Sequential Planetary Gearbox. ASME Paper 85-DET-167, Sept. 1985.

18. Drago, R.J.; and Brown, F.W.: The Analytical and Experimental Evaluation of Resonant Response in High-Speed, Lightweight, Highly Loaded Gearing. ASME Paper 80-C2/DET-22, Aug. 1980.

19. Smith, R.E.: Identification of Gear Noise with Single Flank Composite Measurement, Gear Technology, vol. 3, no. 3, May/June 1986.

20. Harris, T.A.: Rolling Bearing Analysis, 2nd edition, Wiley, 1984, Chapter 7.

TABLE I.—CHARACTERISTICS OF UH-60A TRANSMISSION AT 100-PERCENT
ROTOR SPEED (258 rpm)

(a) Shaft speeds and frequencies and tooth-meshing harmonics

Gear component	Number of teeth	Shaft speed, rpm	Shaft frequency, Hz	First	Second	Third	Fourth
				Tooth-meshing harmonics, Hz			
Spiral-bevel input pinion	22	20 909	348.5	7667	15 334	----	----
Spiral-bevel input gear	80	5 750	95.83	7667	15 334	----	----
Combining bevel pinion	17	5 750	95.83	1629	3 258	4887	6516
Main bevel gear (lower)	81	1 207	20.11	1629	3 258	4887	6516
Sun gear	62	1 207	[a]15.81	980	1 961	2941	3921
Planet gears (five)	83	450.7	[a]11.81	980	1 961	2941	3921
Carrier (output)	---	258.0	4.300	----	----	----	----
Planet passing frequency	---	------	21.50	----	----	----	----
Ring gear	228	0	[a]4.30	980	1 961	2941	3921
Main bevel gear (upper)	116	1 207	20.11	2333	4 666	6999	9332
Tail output shaft gear	34	4 117	68.62	2333	4 666	6999	9332
Oil pump gear	152	258	4.300	654	1 307	1961	2614
Oil pump pinion	12	3 268	54.47	654	1 307	1961	2614

(b) Bearing vibration frequencies

Bearing component	Pitch diameter, mm	Element diameter, mm	Number of elements	Contact angle, deg	Inner race	Outer race	Element spin	Cage spin
					Frequency, Hz			
High-speed input shaft (20 909 rpm)								
Thrust bearing	85	15.9	14	20	2868	2011	451	144
Heel roller	85	16.0	14	---	2899	1980	446	141
Nose roller	75	14.0	14	---	2895	1984	450	142
Intermediate-speed shaft (5750 rpm)								
Clutch bearing	173	10.0	40	---	2027	1806	413	45
Dual taper	106.4	7.4	34	---	1742	1516	343	45
Pinion taper	114	12.5	23	---	1225	979	212	43
Pinion nose	85	14.0	14	---	797	545	123	39
Sun/bevel shaft (1207 rpm)								
Upper roller	225	15.0	34	---	365	319	75	9.4
Dual taper	219	11.2	50	---	529	477	98	9.5
Planet gears (450.7 rpm)								
Spherical	140	19.5	18	---	77	58	13	3.2
Main rotor shaft (258.0 rpm)								
Upper roller	190	16.0	30	---	70	59	13	2.0
Duplex ball	160	27.0	16	37.5	39	30	6.3	1.9
Tail output shaft (4117 rpm)								
Inner tapered	72.6	6.06	33	---	1227	1038	204	31
Outer tapered	66	6.06	27	---	1011	841	185	31

[a]Shaft frequencies for sidebands are given relative to carrier frequency.

TABLE II.—TEST POINTS USED FOR VIBRATION AND EFFICIENCY MEASUREMENTS

Escort II reading[a]	Speed, percent of rated	Torque, percent of rated	Power. percent of rated
3	100	28	28
11	99	37	37
16	↑	27	27
17	│	101	100
18	│	77	76
19	↓	54	53
20	73	105	77
21	73	76	55
22	74	51	38
23	75	26	20
25	100	25	25
26	75	25	19
28	50	25	13
29	↑	50	25
30	│	74	37
31	↓	100	50
33	49	76	37
34	75	75	56
35	75	74	56
36	99	75	74
37	99	100	99
38	75	100	75
39	76	50	38
40	99	50	50
45	99	100	99
46	99	74	73
61	100	99	98
62	75	99	74
63	50	100	49
64	100	75	74
65	75	↑	56
66	52	│	39
67	51	↓	38
68	100	25	25
69	75	25	19
70	75	50	37
71	99	50	50
72	49	50	25
73	99	99	98
74	75	100	75
75	50	100	50
77	99	74	73
78	99	51	50
79	75	75	56
80	50	75	37
81	75	50	38
82	50	50	25
83	99	25	25
84	75	27	20

[a]Efficiency data points taken at readings 61 to 65 and 67 to 84. Vibration data points taken at all readings listed

8
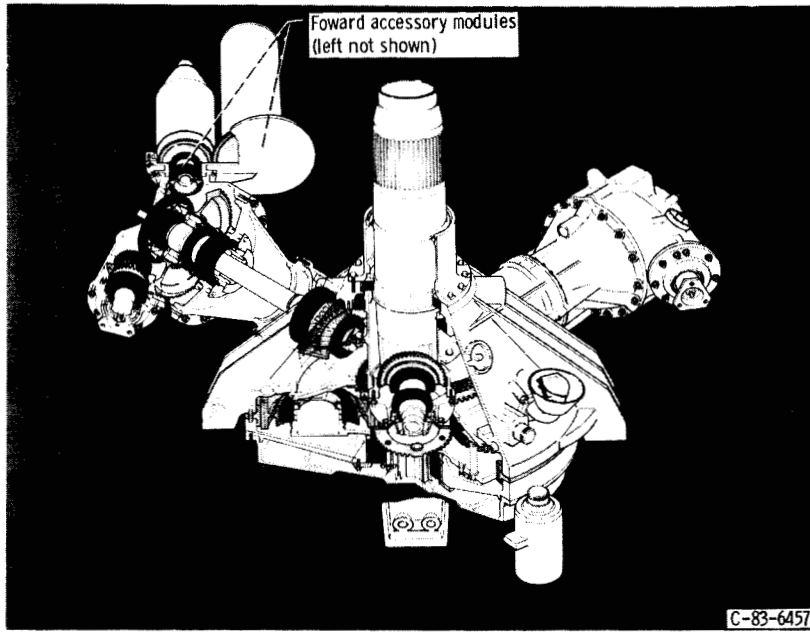
Figure 1.—Isometric section view of UH–60A helicopter transmission.

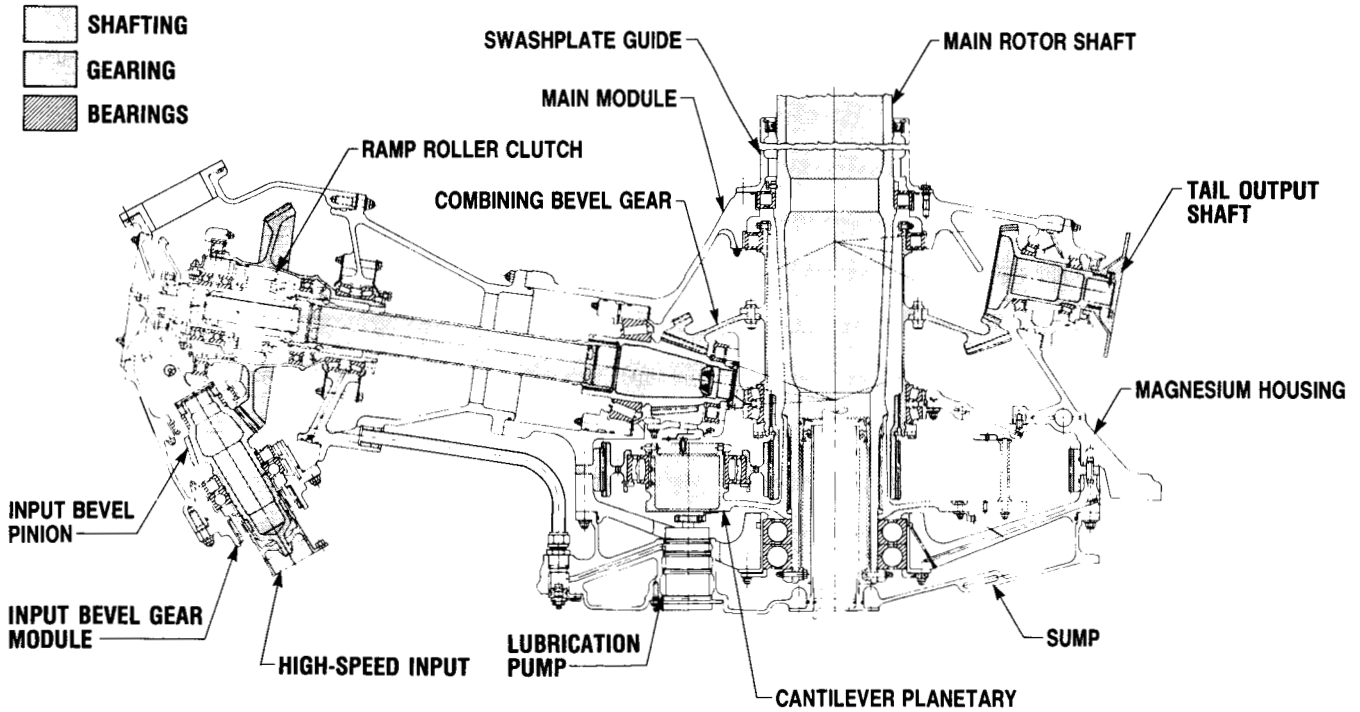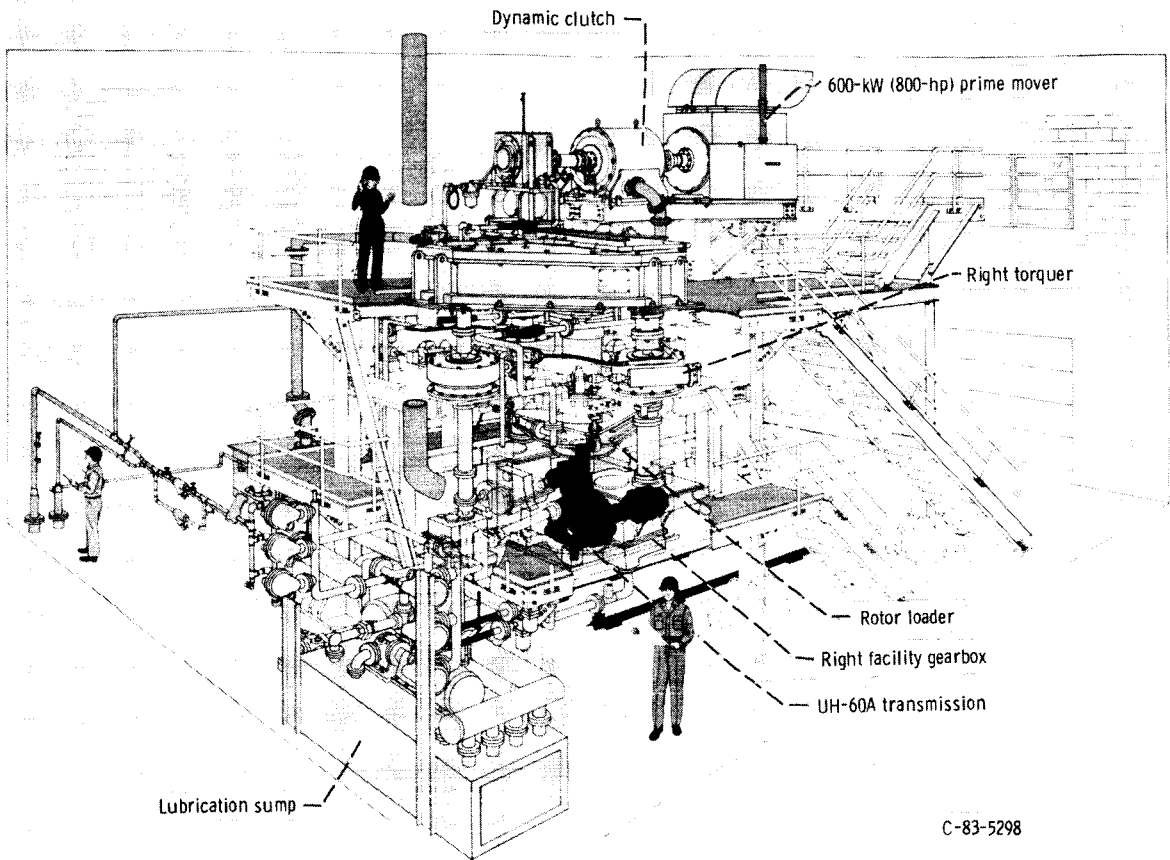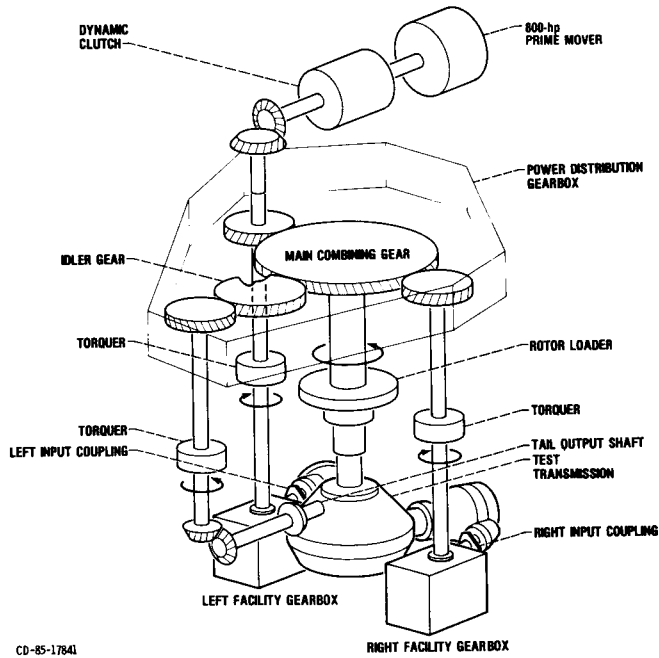Figure 2.—Section view of UH–60A helicopter transmission along input module and tail.

9

Figure 3.—NASA Lewis 2240-kW (3000-hp) helicopter transmission test stand.

Figure 4.—Schematic of 2240-kW (3000-hp) helicopter transmission test stand.
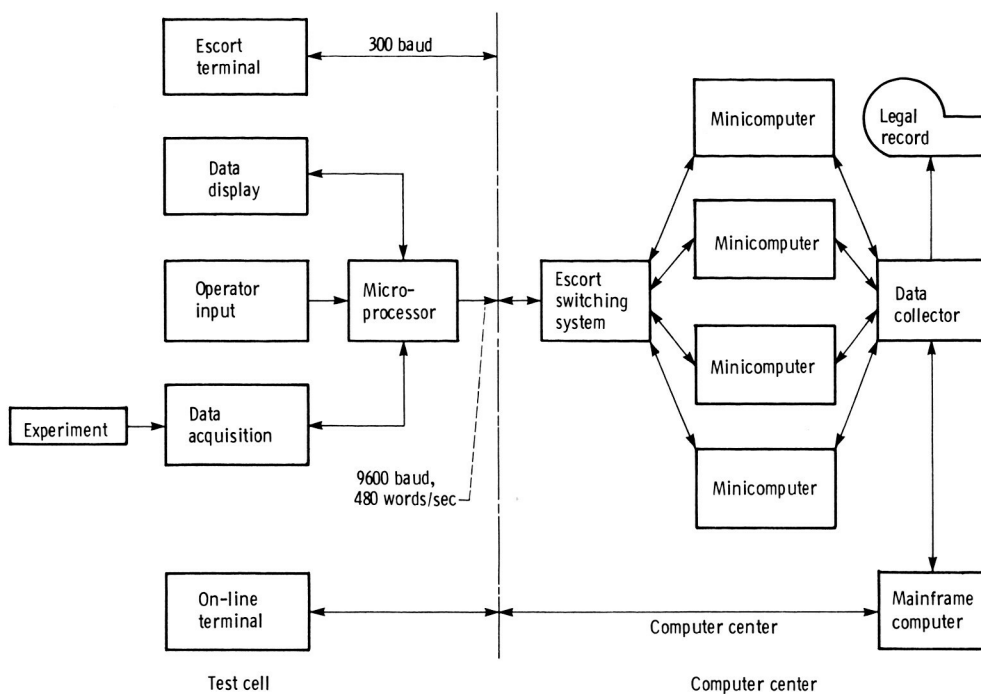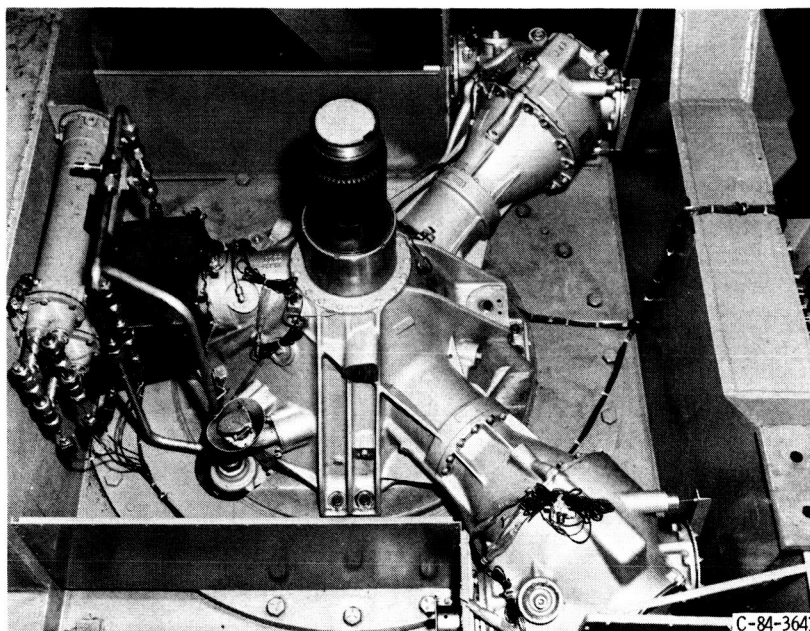
Figure 5.—Escort II data acquisition system.

Figure 6.—Top view of uninsulated UH–60A transmission.
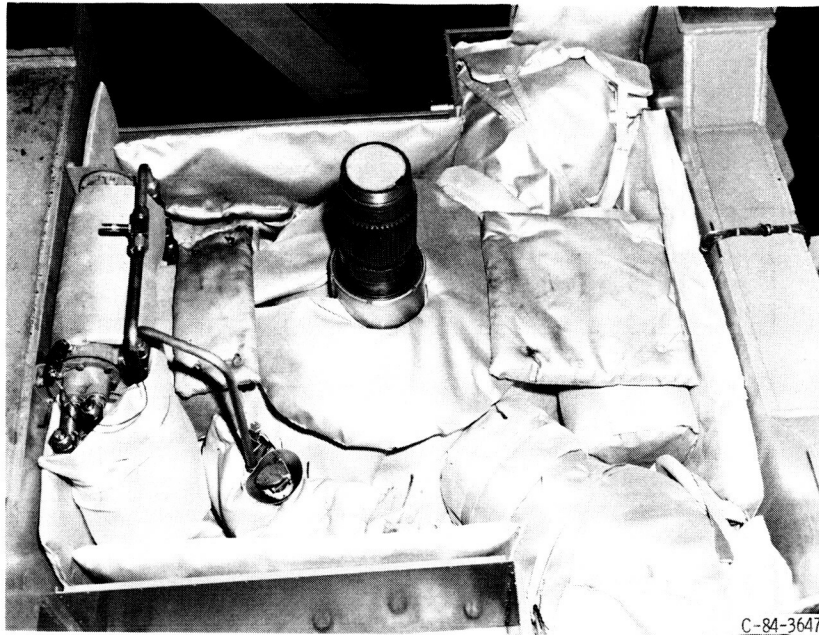
11

C-84-3647

Figure 7.—Top view of UH-60A transmission with insulation blankets installed.
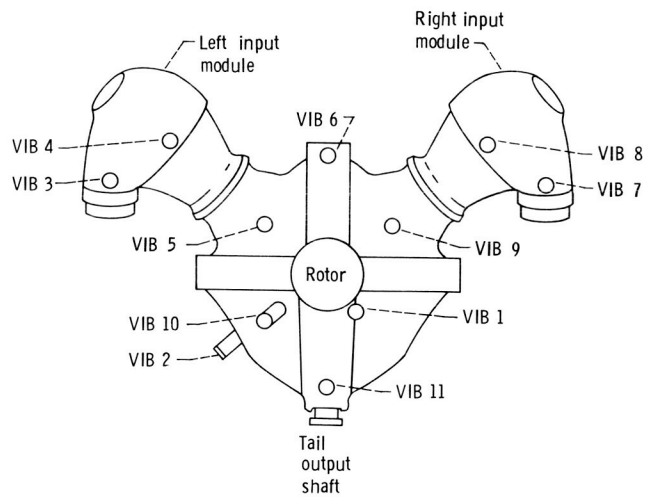

Figure 8.—Locations of accelerometers on UH-60A transmission. All accelerometers mounted vertically except VIB 2 (horizontal) and VIB 10 (33° from vertical).
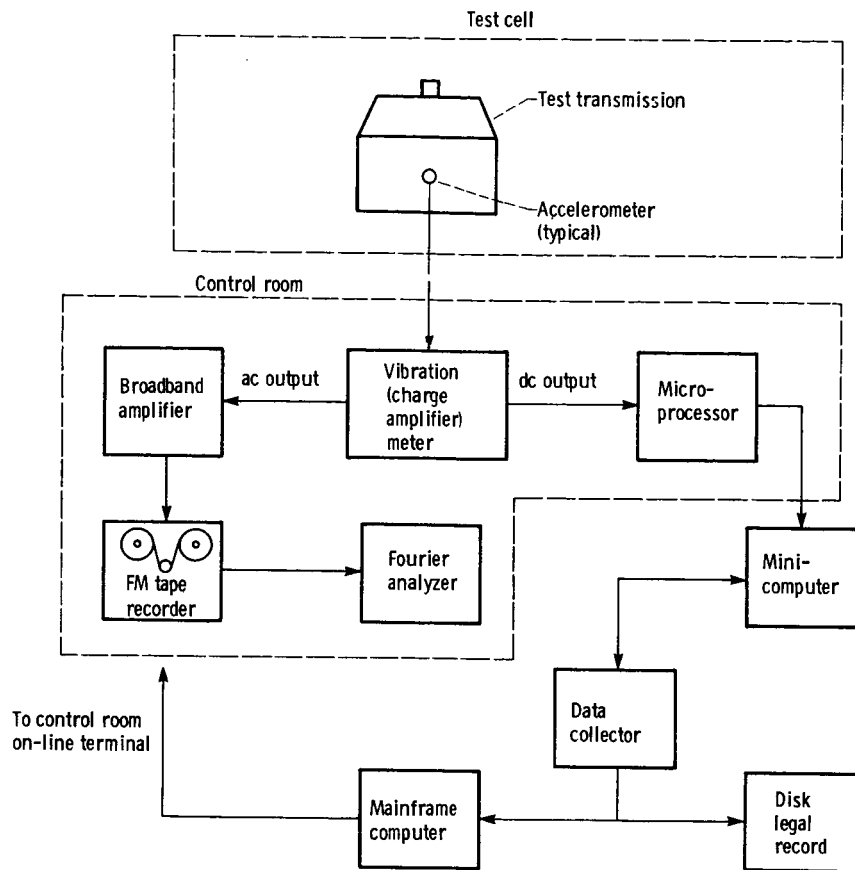
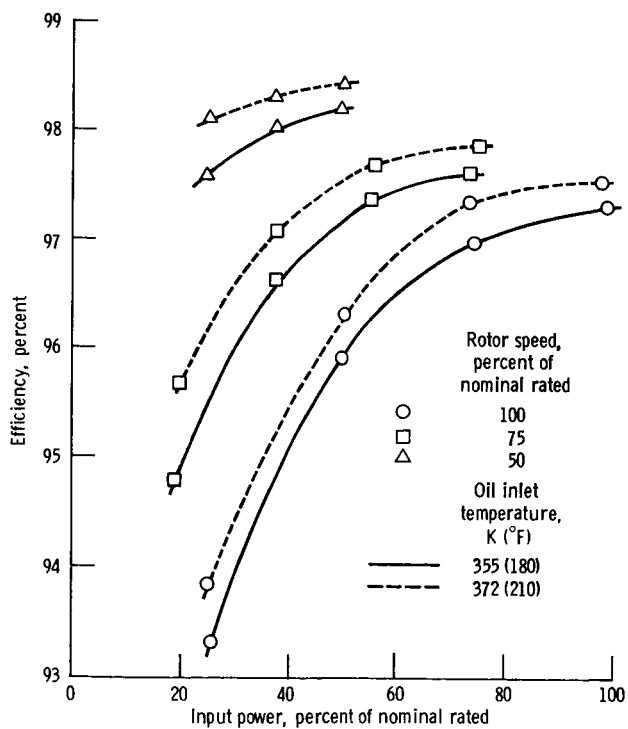Figure 9.—Vibration measurement system.

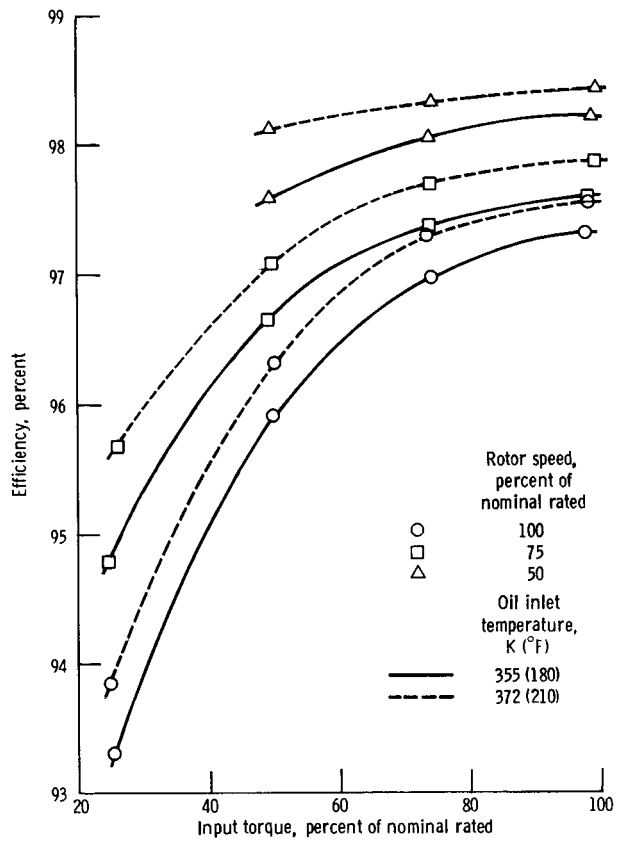Figure 10.—Mechanical efficiency of UH-60A as function of input power.

Figure 11.—Mechanical efficiency of UH-60A as function of input torque.
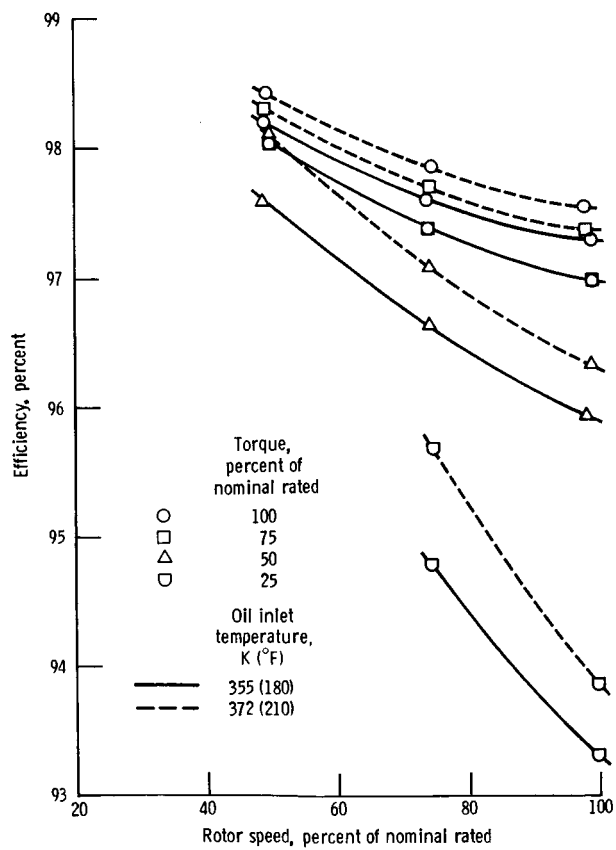
Figure 12.—Mechanical efficiency of UH-60A as function of rotor speed.
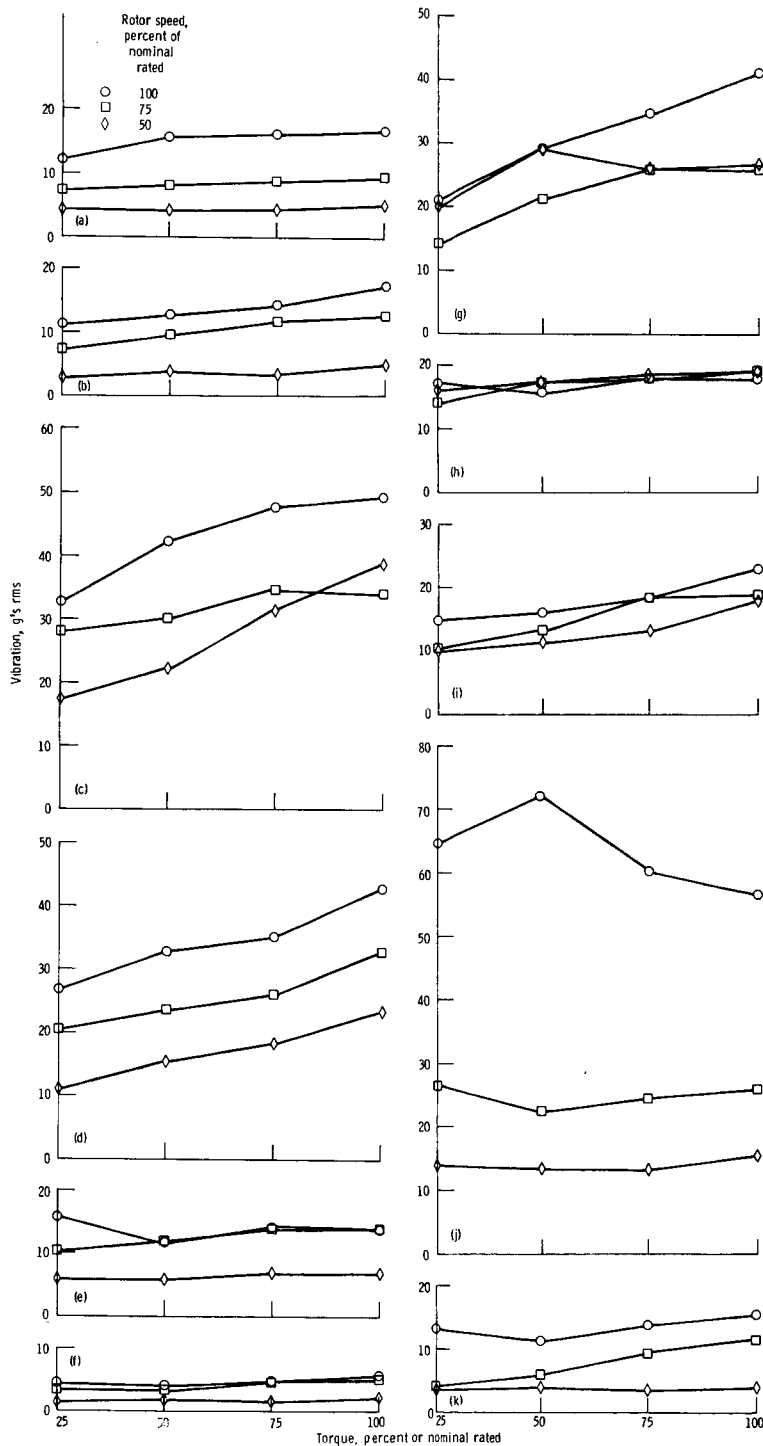
(a) VIB 1, main rotor bearing (vertical).
(b) VIB 2, ring gear (radial-horizontal).
(c) VIB 3, left input pinion (radial-vertical).
(d) VIB 4, left input gear (radial-vertical).
(e) VIB 5, left combining pinion (radial-vertical).
(f) VIB 6, front mounting foot (vertical).

(g) VIB 7, right input pinion (radial-vertical).
(h) VIB 8, right input gear (radial-vertical).
(i) VIB 9, right combining pinion (radial-vertical).
(j) VIB 10, upper housing side wall (radial).
(k) VIB 11, tail output shaft (radial vertical).

Figure 13.—Vibration amplitude as function of rotor speed and torque.
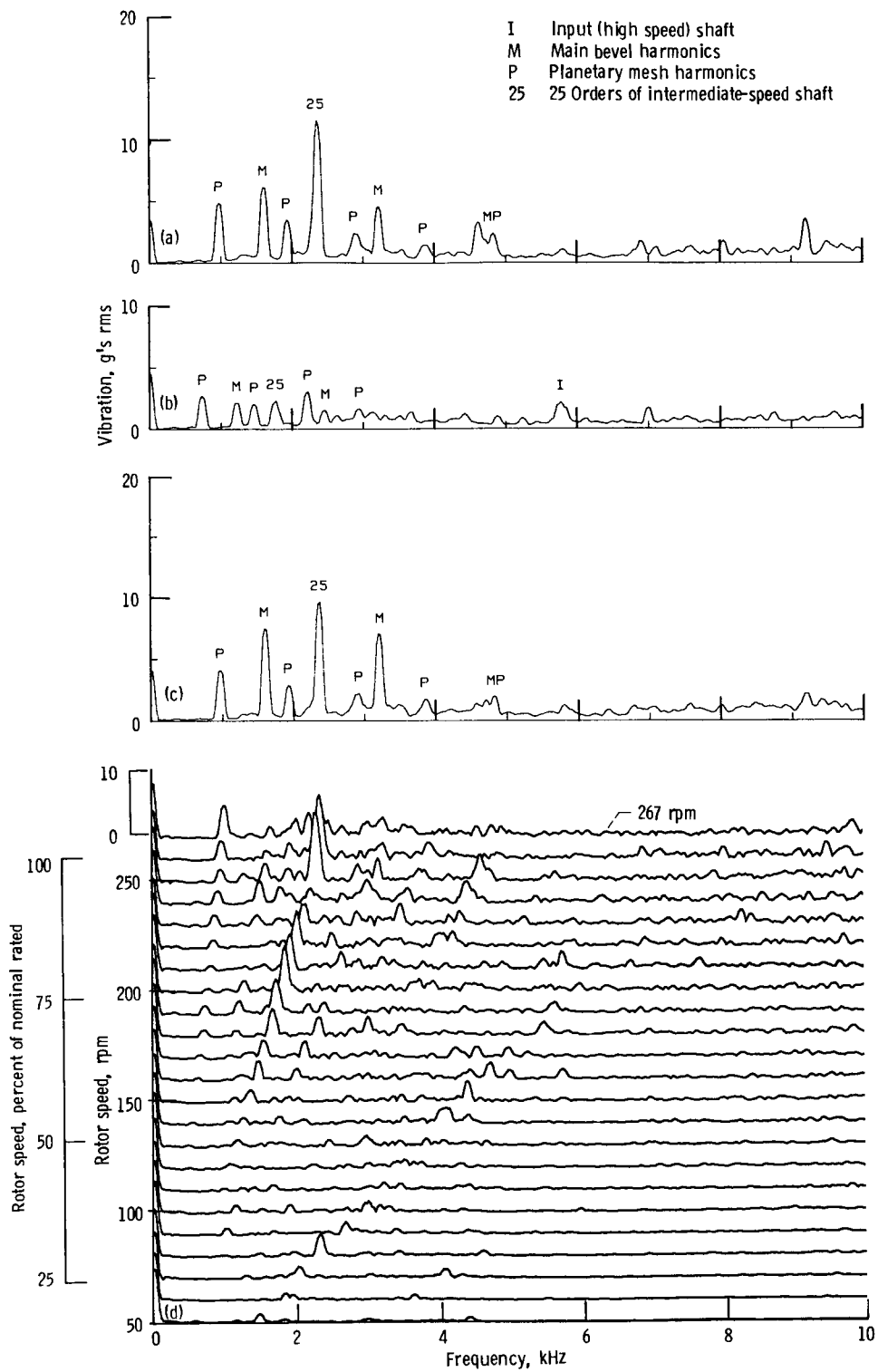
15

(a) Spectrum for 99-percent speed and 99-percent torque.
(b) Spectrum for 75-percent speed and 100-percent torque.
(c) Spectrum for 99-percent speed and 74-percent torque.
(d) Speed map for 25-percent torque and 19- to 103-percent speed.

Figure 14.—Vibration spectra and speed map for VIB 1 (main rotor bearing).

M   Main bevel harmonics
P   Planetary mesh harmonics
25   25 Orders of intermediate-speed shaft

Vibration, g's rms

Rotor speed, percent of nominal rated

Rotor speed, rpm

267 rpm

Frequency, kHz

(a) Spectrum for 99-percent speed and 99-percent torque.
(b) Spectrum for 75-percent speed and 100-percent torque.
(c) Spectrum for 99-percent speed and 74-percent torque.
(d) Speed map for 25-percent torque and 19- to 103-percent speed.

Figure 15.—Vibration spectra and speed map for VIB 2 (ring gear).

I   Input (high speed) shaft
S   Sidebands of input shaft
25   25 Orders of intermediate speed shaft
10   10 Orders of high-speed shaft
-    Difference frequency: I - 25
+   Sum frequency: I + 25

(a) Spectrum for 99-percent speed and 99-percent torque.
(b) Spectrum for 75-percent speed and 100-percent torque.
(c) Spectrum for 99-percent speed and 74-percent torque.
(d) Speed map for 25-percent torque and 19- to 103-percent speed.

Figure 16.—Vibration spectra and speed map for VIB 3 (left input pinion).

(a) Spectrum for 99-percent speed and 99-percent torque.
(b) Spectrum for 75-percent speed and 100-percent torque.
(c) Spectrum for 99-percent speed and 74-percent torque.
(d) Speed map for 25-percent torque and 19- to 103-percent speed.

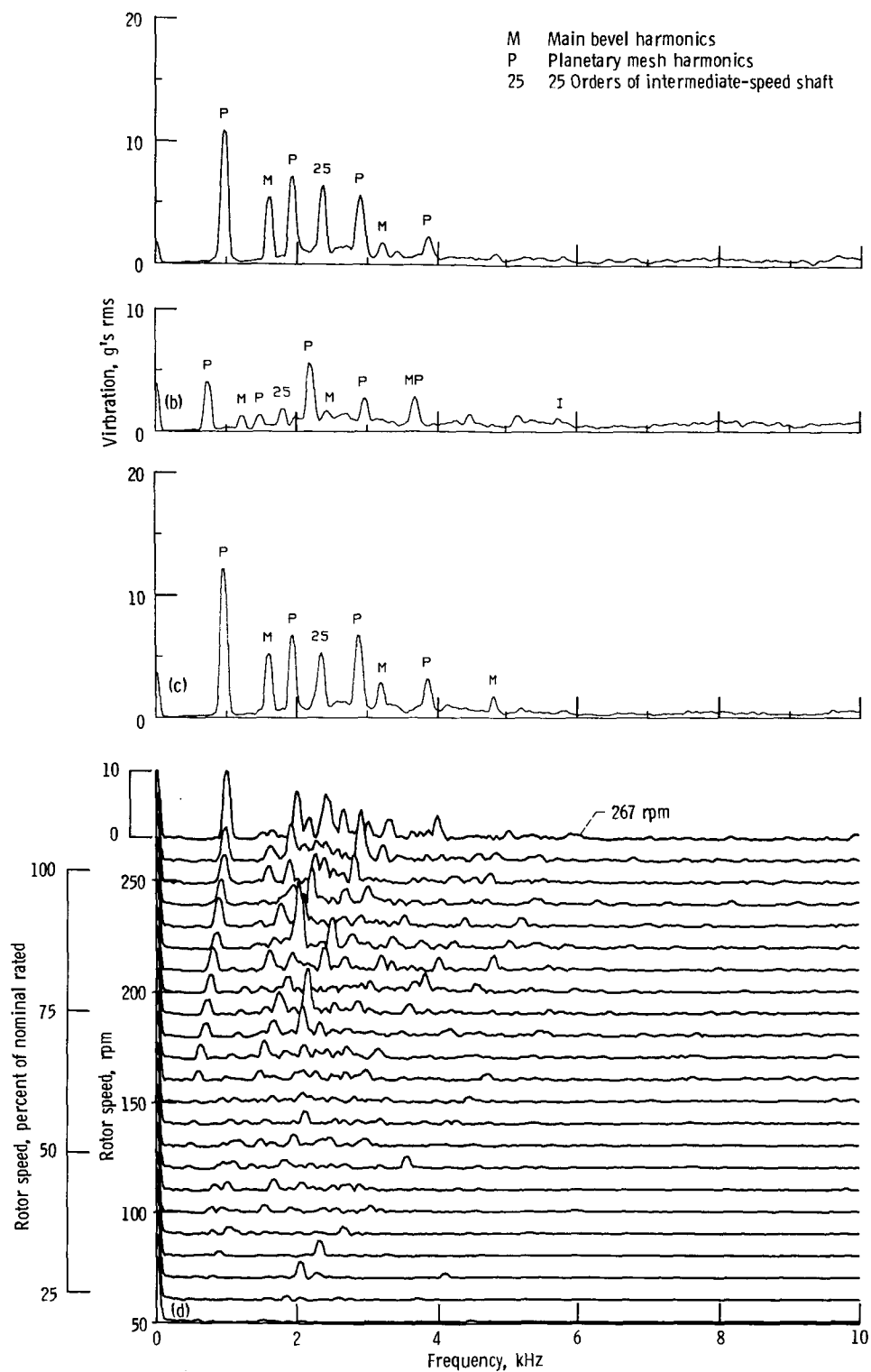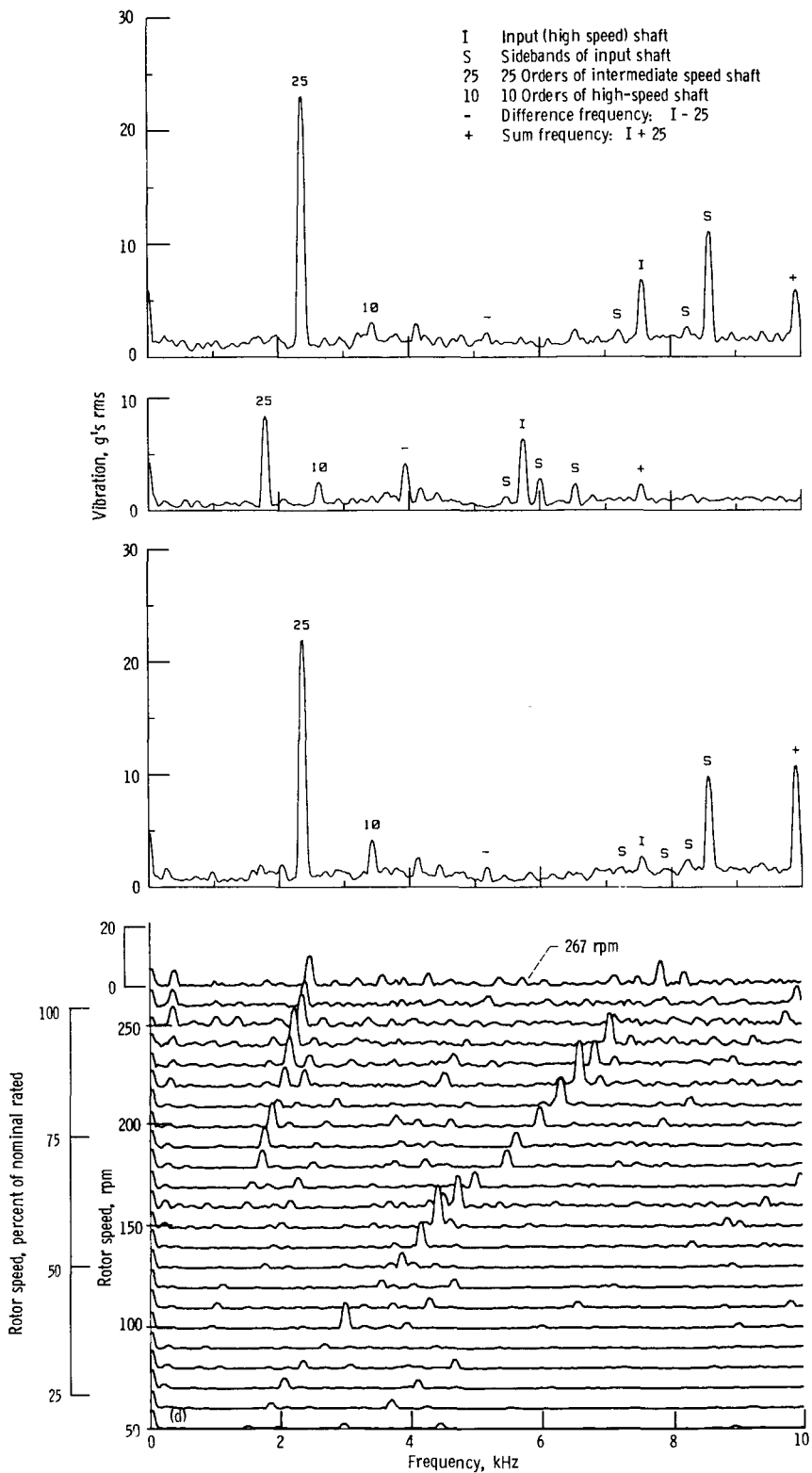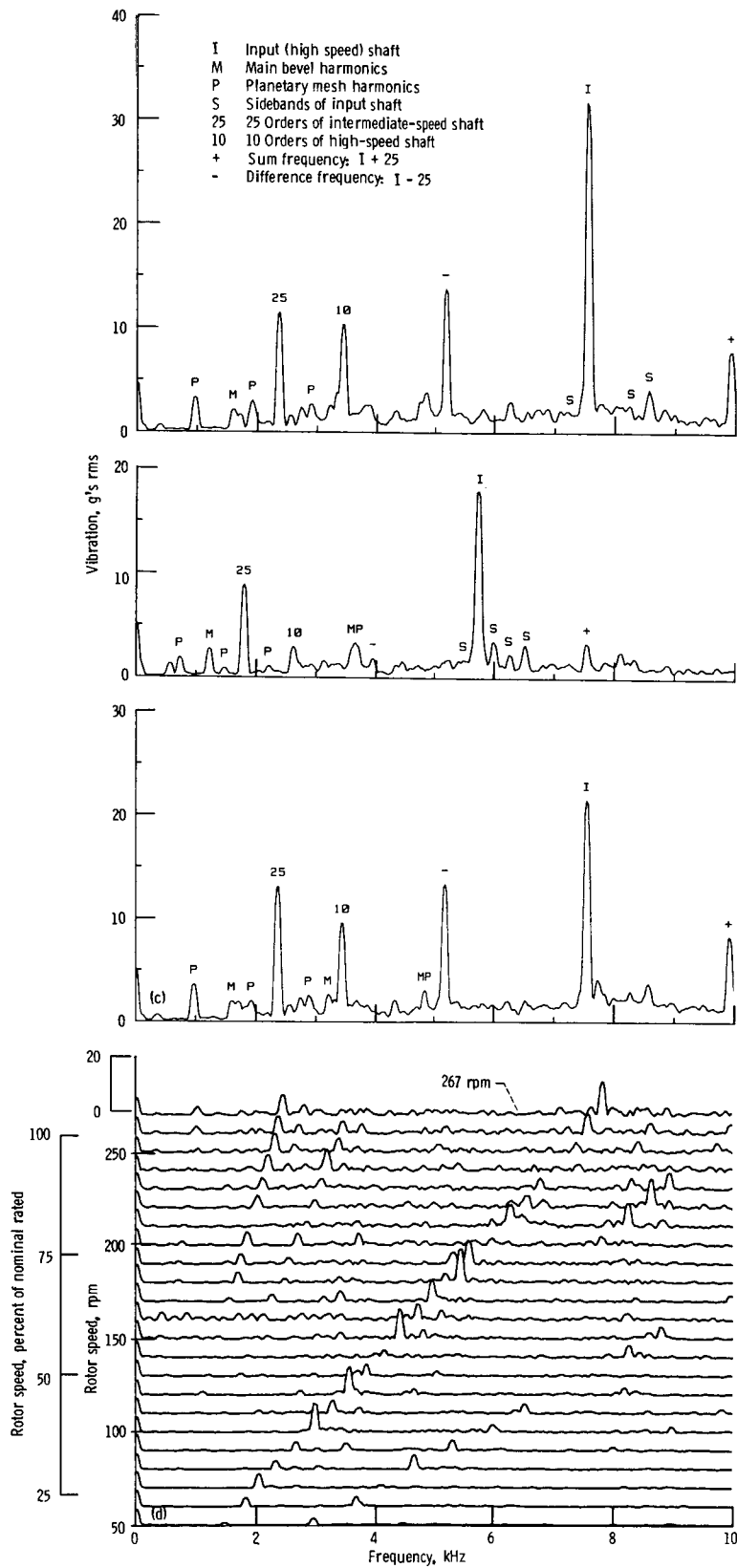Figure 17.—Vibration spectra and speed map for VIB 4 (left input gear).

I   Input (high speed) shaft
M   Main bevel harmonics
P   Planetary mesh harmonics
25   25 Orders of intermediate-speed shaft

(a) Spectrum for 99-percent speed and 99-percent torque.
(b) Spectrum for 75-percent speed and 100-percent torque.
(c) Spectrum for 99-percent speed and 74-percent torque.
(d) Speed map for 25-percent torque and 19- to 103-percent speed.

Figure 18.—Vibration spectra and speed map for VIB 5 (left combining pinion).

M   Main bevel harmonics
P   Planetary mesh harmonics
25   25 Orders of intermediate-speed shaft

(a) Spectrum for 99-percent speed and 99-percent torque.
(b) Spectrum for 75-percent speed and 100-percent torque.
(c) Spectrum for 99-percent speed and 74-percent torque.
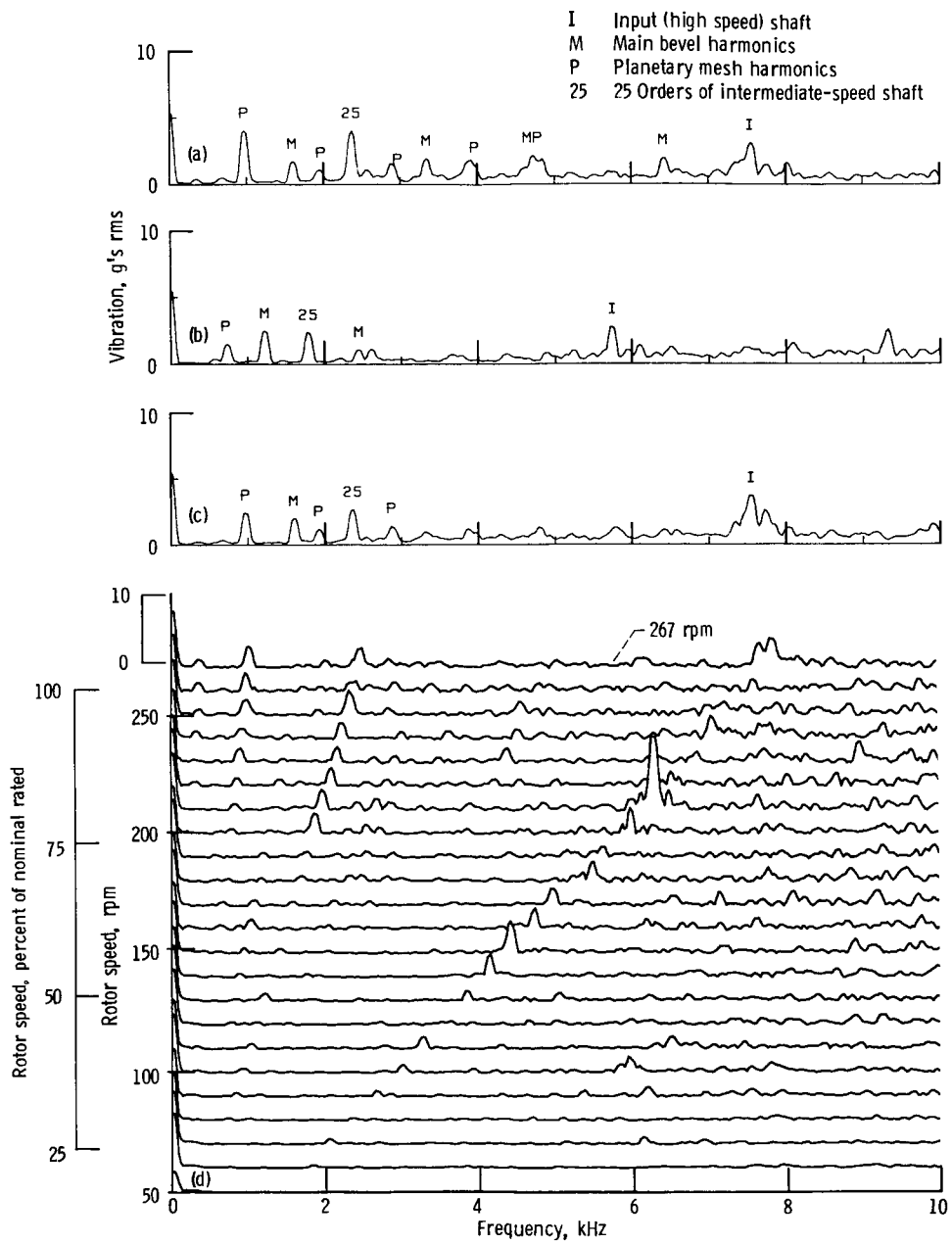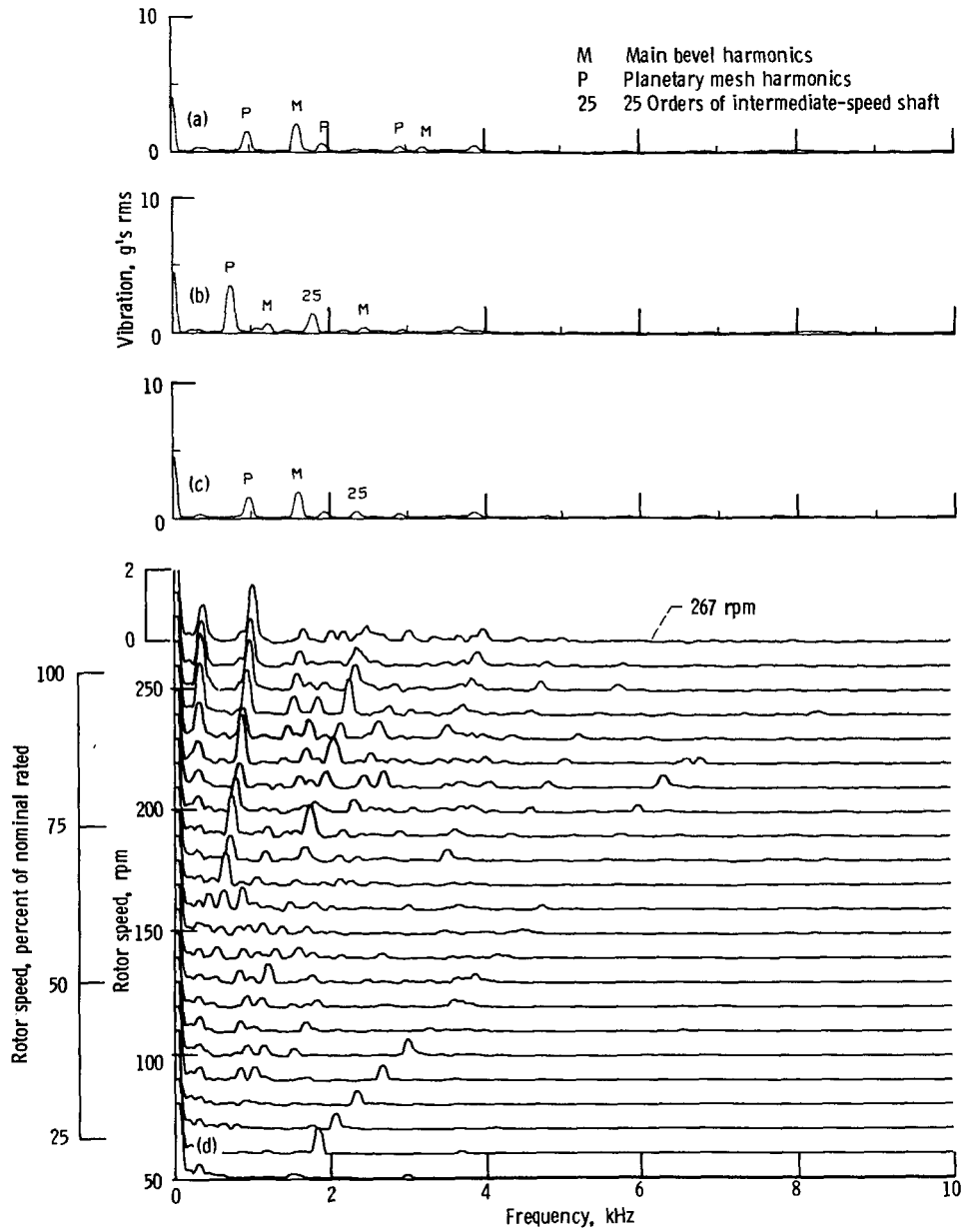(d) Speed map for 25-percent torque and 19- to 103-percent speed.

Figure 19.—Vibration spectra and speed map for VIB 6 (front mounting foot).

(a) Spectrum for 99-percent speed and 99-percent torque.
(b) Spectrum for 75-percent speed and 100-percent torque.
(c) Spectrum for 99-percent speed and 74-percent torque.
(d) Speed map for 25-percent torque and 19- to 103-percent speed.

Figure 20.—Vibration spectra and speed map for VIB 7 (right input pinion).

I   Input (high speed) shaft
M   Main bevel harmonics
P   Planetary mesh harmonics
25 25 Orders of intermediate-speed shaft
10 10 Orders of high-speed shaft

(a) Spectrum for 99-percent speed and 99-percent torque.
(b) Spectrum for 75-percent speed and 100-percent torque.
(c) Spectrum for 99-percent speed and 74-percent torque.
(d) Speed map for 25-percent torque and 19- to 103-percent speed.

Figure 21.—Vibration spectra and speed map for VIB 8 (right input gear).

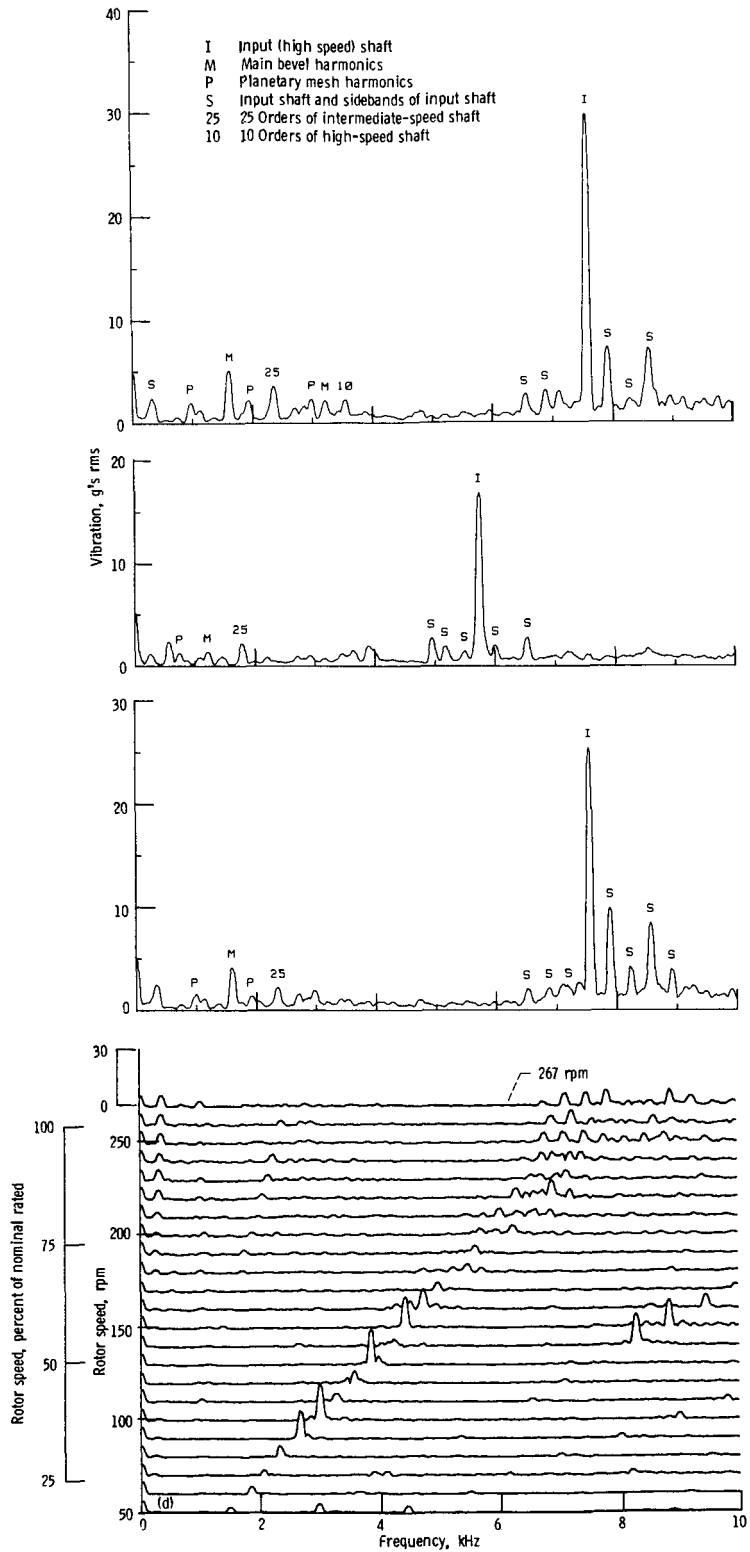23

I   Input (high speed) shaft
M   Main bevel harmonics
P   Planetary mesh harmonics
S   Sidebands of input shaft
25   25 Orders of intermediate-speed shaft

Vibration, g's rms

Rotor speed, percent of nominal rated

Rotor speed, rpm

267 rpm

Frequency, kHz

(a) Spectrum for 99-percent speed and 99-percent torque.
(b) Spectrum for 75-percent speed and 100-percent torque.
(c) Spectrum for 99-percent speed and 74-percent torque.
(d) Speed map for 25-percent torque and 19- to 103-percent speed.

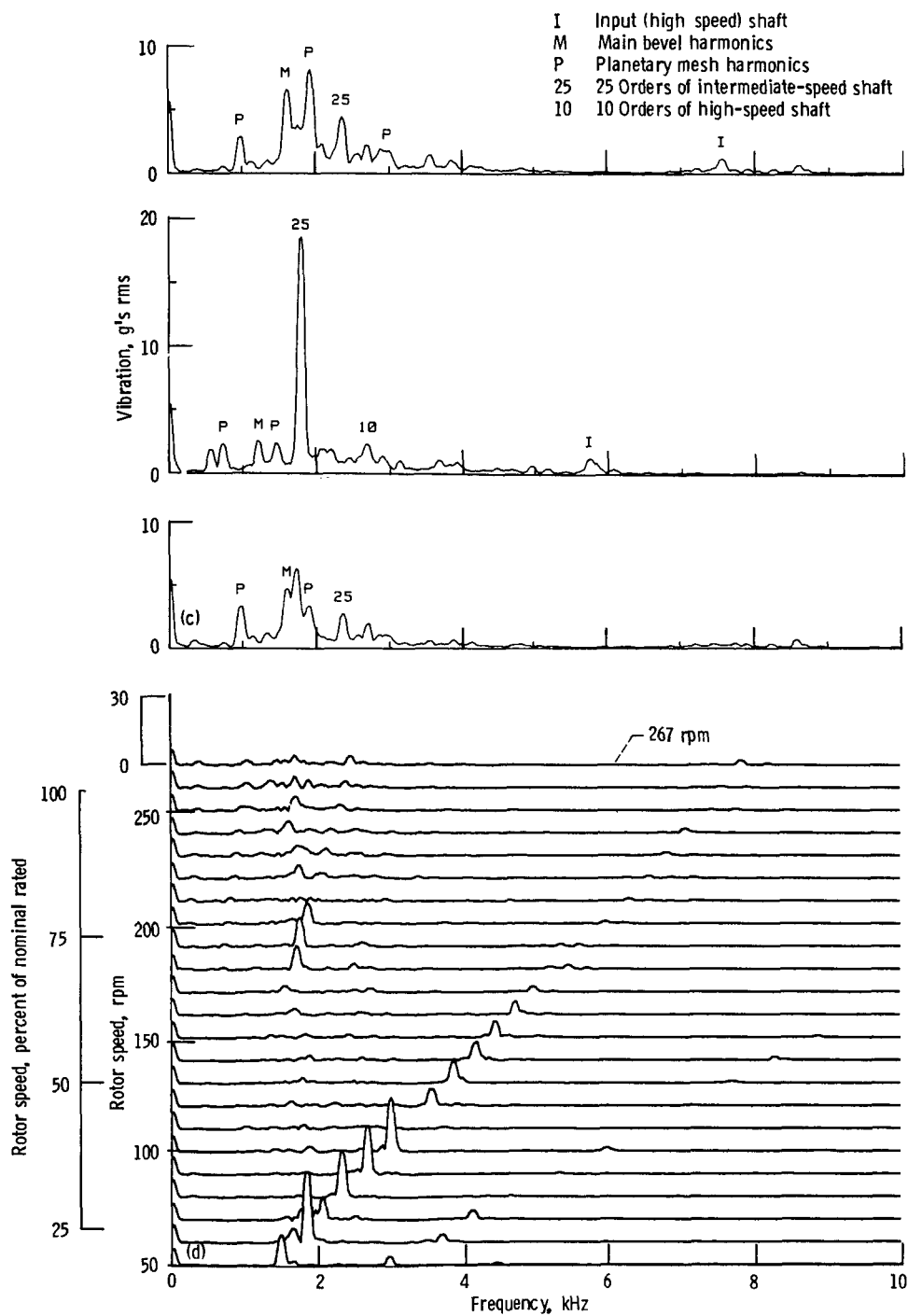Figure 22.—Vibration spectra and speed map for VIB 9 (right combining pinion).

I   Input (high speed) shaft
M   Main bevel harmonics
P   Planetary mesh harmonics
25 25 Orders of intermediate-speed shaft

Vibration, g's rms

Rotor speed, percent of nominal rated

Rotor speed, rpm

267 rpm

Frequency, kHz

(a) Spectrum for 99-percent speed and 99-percent torque.
(b) Spectrum for 75-percent speed and 100-percent torque.
(c) Spectrum for 99-percent speed and 74-percent torque.
(d) Speed map for 25-percent torque and 19- to 103-percent speed.

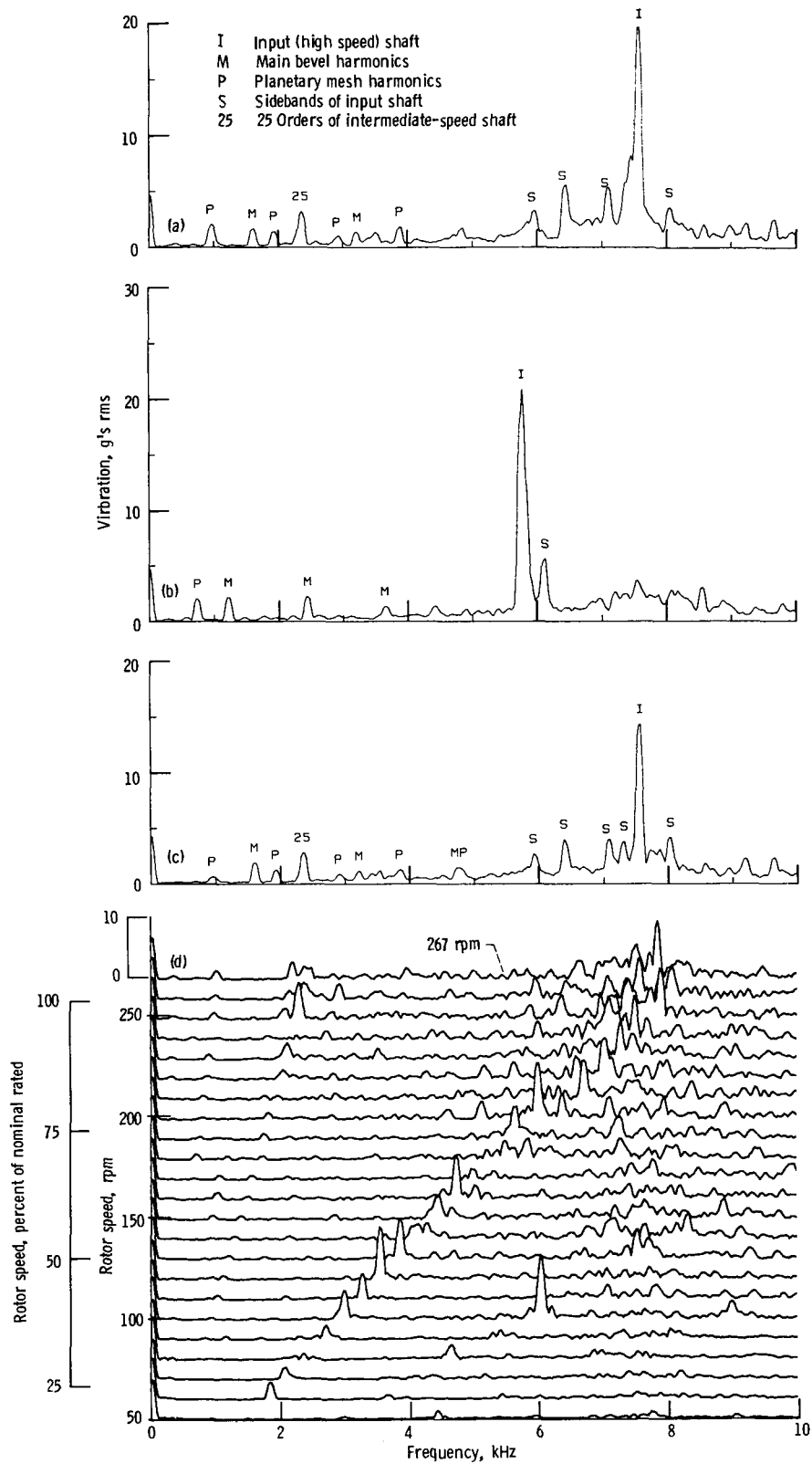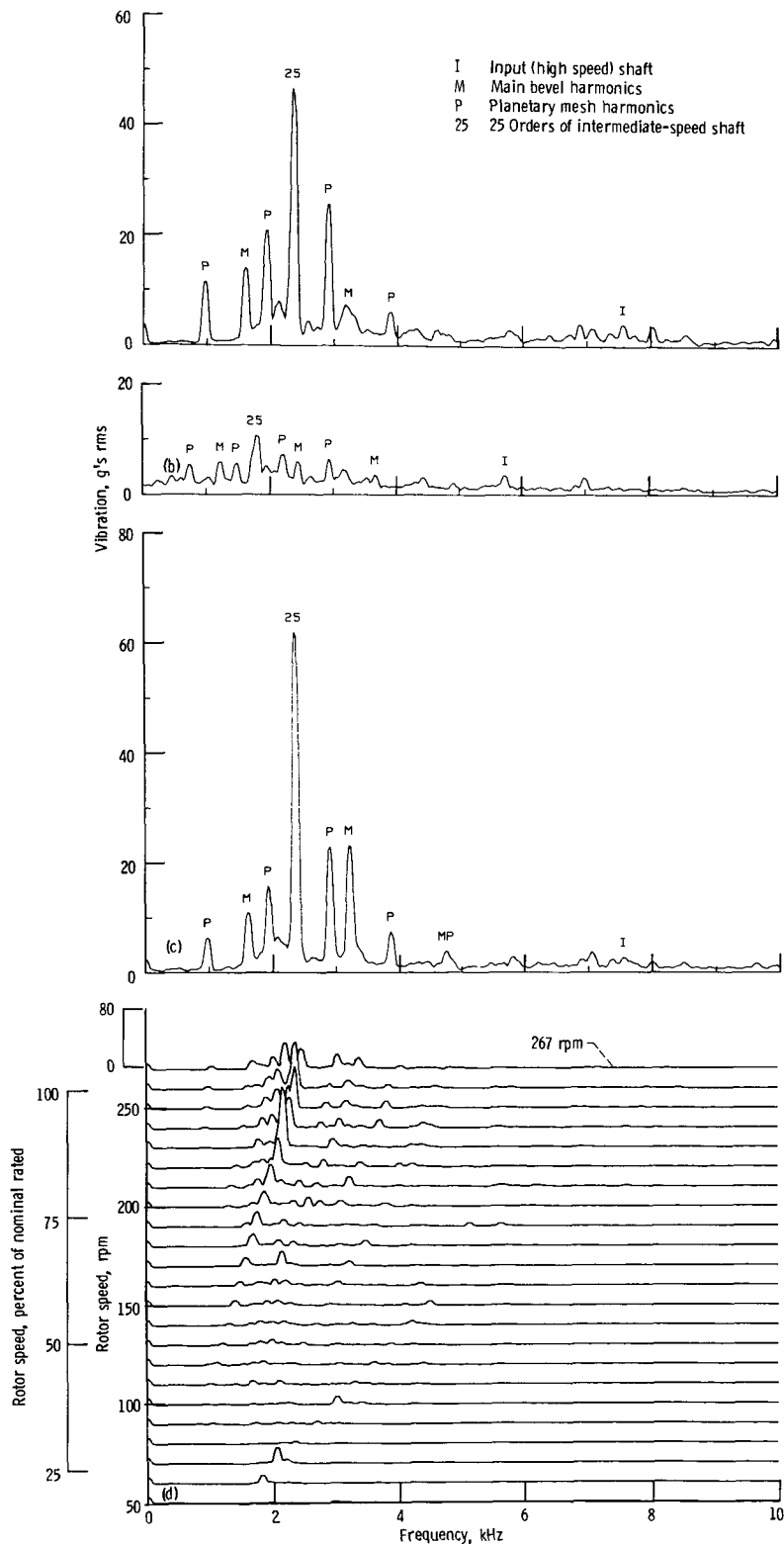Figure 23.—Vibration spectra and speed map for VIB 10 (upper housing side wall).

(a) Spectrum for 99-percent speed and 99-percent torque.
(b) Spectrum for 75-percent speed and 100-percent torque.
(c) Spectrum for 99-percent speed and 74-percent torque.
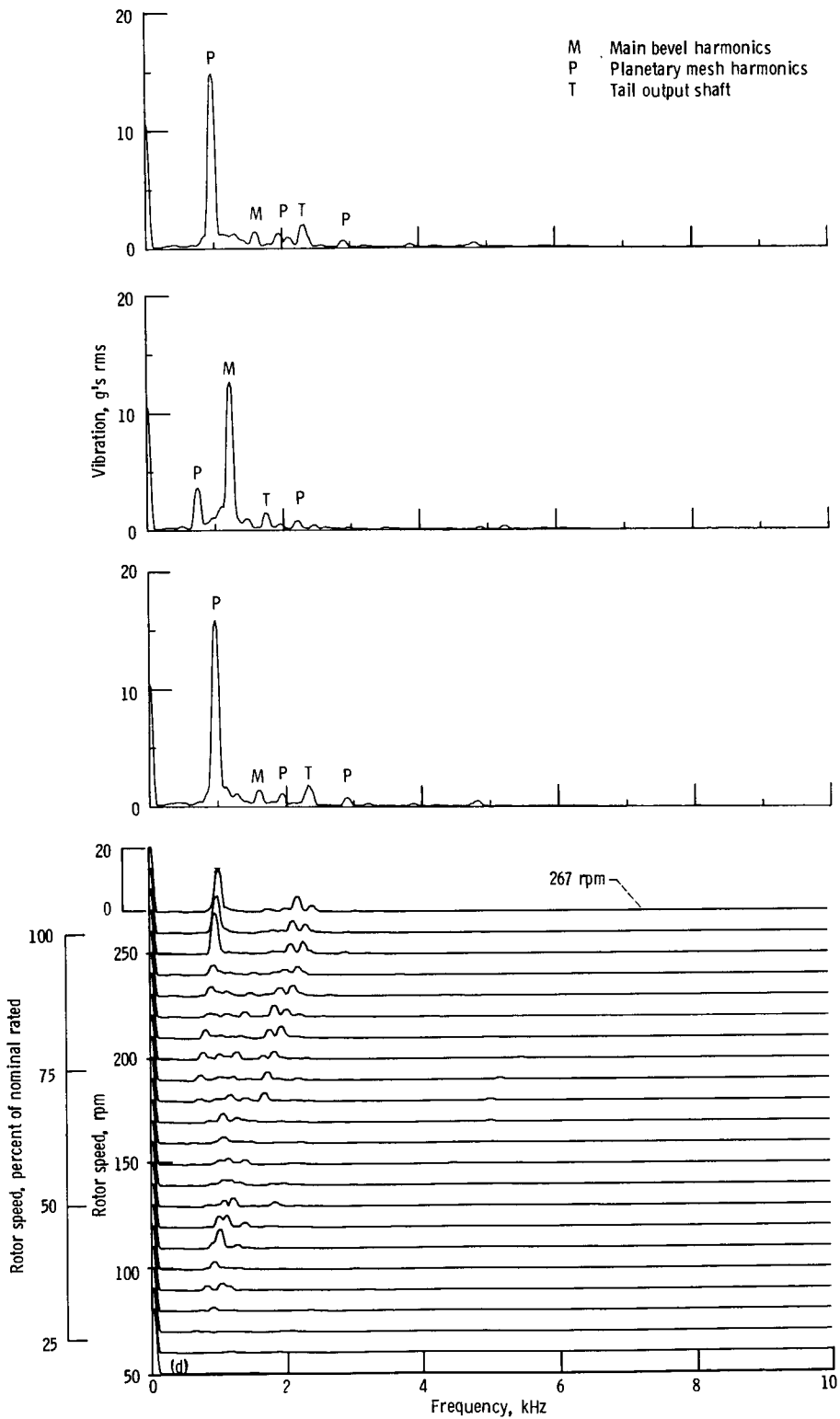(d) Speed map for 25-percent torque and 19- to 103-percent speed.

Figure 24.—Vibration spectra and speed map for VIB 11 (tail output shaft).

Figure 25.—Left spiral-bevel input pinion for UH-60A transmission.

1. Report No.	2. Government Accession No.	3. Recipient's Catalog No.
NASA TP-2626		

4. Title and Subtitle	5. Report Date
Testing of UH-60A Helicopter Transmission in NASA Lewis 2240-kW (3000-hp) Facility	August 1986
	6. Performing Organization Code
	505-62-51

7. Author(s)	8. Performing Organization Report No.
Andrew M. Mitchell, Fred B. Oswald, and Harold H. Coe	E-2941
	10. Work Unit No.

9. Performing Organization Name and Address	11. Contract or Grant No.
National Aeronautics and Space Administration Lewis Research Center Cleveland, Ohio 44135	
	13. Type of Report and Period Covered

12. Sponsoring Agency Name and Address	Technical Paper
National Aeronautics and Space Administration Washington, D.C. 20546	14. Sponsoring Agency Code

15. Supplementary Notes

16. Abstract

The U.S. Army's UH-60A Black Hawk 2240-kW (3000-hp) class, twin-engine helicopter transmission was tested at the NASA Lewis Research Center. The vibration and efficiency test results will be used to enhance the data base for similar-class helicopters. Most of the data were obtained for a matrix of test conditions of 50 to 100 percent of rated rotor speed and 20 to 100 percent of rated input power. The transmission's mechanical efficiency at 100 percent of rated power was 97.3 and 97.5 percent with its inlet oil maintained at 355 and 372 K (180 and 210 °F), respectively. The highest vibration reading was 72 g's rms at the upper housing side wall. Other vibration levels measured near the gear meshes are reported.

17. Key Words (Suggested by Author(s))	18. Distribution Statement
Helicopter transmission Vibration Efficiency	Unclassified – unlimited STAR Category 37

19. Security Classif. (of this report)	20. Security Classif. (of this page)	21. No. of pages	22. Price*
Unclassified	Unclassified	27	A03

*For sale by the National Technical Information Service, Springfield, Virginia 22161